PEOPLE'S DEMOCRATIC REPUBLIC OF ALGERIA

MINISTRY OF HIGHER EDUCATION AND SCIENTIFIC RESEARCH

UNIVERSITY OF MOHAMED BOUDIAF - M'SILA

FACULTY OF SCIENCE

PHYSICS DEPARTMENT

Nº. Ph/MAT/05/2023

FIELD: Materials science

SECTOR: Physics

OPTION: Physics of Materials

Dissertation submitted for obtaining academic Master's degree

Presented by: Fahima DJELLAL

Title

Sol-Gel Preparation and characterization of nanocrystalline $La_{(1-x)}Mg_xMnO_3$ perovskite

Defended on 24/06/2023 before the jury composed of:

President:	Dr. Ameur Ouali	University of Mohamed Boudiaf- M'sila
Supervisor:	Dr. Foudil Sahnoune	University of Mohamed Boudiaf- M'sila
Co-Supervisor:	Dr. Amar Djemli	University of Mohamed Boudiaf- M'sila
Examiner:	Dr. Abdelmadjid Boussendel	University of Mohamed Boudiaf- M'sila
Examiner:	Dr. Nadjib Baadji	University of Mohamed Boudiaf- M'sila

Academic Year: 2022/2023

Dedicates

To my parents, may God give them

health and long life...

To my dear sisters

To all my friends, especially my friend Fawzia

To all my teachers

To all those who are dear to me...

Fahima

Acknowledgements

First and foremost, all praise of gratitude and thankfulness is due to **ALLAH** the Almighty for all the bounties he bestowed on me beyond my expectations. Then, peace and blessings of Allah be upon His Messenger **Mohammed** , who says: "Whoever does not thank people (for their favours) is not thankful to **Allah**".

I would like to thank all who encouraged me to follow this path and motivated me to keep going.

Foremost, the heart of these acknowledgments goes to my supervisor, Pr. **SAHNOUNE Foudil**. The information and insights you provided me with were invaluable. I have benefited greatly from your experience and extensive knowledge, and you have always been willing to offer assistance and guidance at every step. Thank you again for everything you have provided and for the time and effort you have dedicated. It is an honor for me that Pr. **OUALI Ameur** has accepted to chair the jury. My sincere thanks go to Pr. **BOUSSENDEL Abdelmadjid** and Pr. **BAADJI Nadjib** for accepting to participate as an examiner in this jury. Special thanks to Dr. **DJEMLI Amar,** Co-Supervisor for his invaluable assistance and valuable advice in completing my master's thesis.

We would like to extend our deepest gratitude and appreciation to Pr**. DHAHRI Essebti** Department of Physics, University of Sfax, who has stood by our side and enlightened us with his knowledge and experience. We are thankful for his valuable educational guidance and the continuous encouragement that has inspired us to reach our highest potential. We greatly appreciate the dedication and flexibility that has beendemonstrated in assisting us, despite the geographical distance. His interest and insightful responses to our questions have been a rich source of knowledge and learning. We cherish our academic experience and feel grateful for his participation in our scholarly journey. This work is a product of that journey, and this project would not have been possible without his invaluable efforts and contributions. With all love and respect, we extend our thanks for the commitment and support he has provided us during this period. Our hope is to continue learning and growing under his supervision in the future.

Last but not least, I would like to express my sincere appreciation to Dr. **HERAIZ Menad** for his valuable advices.

CONTENTS

General Iintroduction

Perovskite compounds are a significant area of study in the field of materials science and applied physics. They are distinguished by their unique three-dimensional crystalline structure and possess a wide range of noteworthy properties, such as superconductivity, semiconductor, ferroelectric insulation, and many others. These properties vary depending on the specific elements and structure of the compound.

Among the essential properties, magneto-thermal properties have gained considerable importance. The majority of materials used in this field are based on gadolinium, which is an element classified as both rare and precious. Gadolinium is not abundantly distributed in the Earth's crust, making its extraction and production challenging and expensive. The escalating demand for gadolinium raises concerns about the depletion of its resources. Consequently, researchers have been exploring alternative materials.

One such intriguing alternative is the compound $LaMnO_3$, which stands out as a prominent example of perovskite materials. Studies have demonstrated that doping $LaMnO_3$ with elements such as strontium (Sr) and calcium (Ca) introduces significant magneto-thermal properties, making it suitable for applications in magnetic cooling. As a result, we conducted the synthesis of $LaMnO_3$ doped with magnesium (Mg) using a sol-gel method at various concentrations.

This research aims to investigate the potential of Mg-doped $LaMnO_3$ and its suitability for utilization in magneto-thermal applications, thereby addressing the concerns surrounding the limited availability and high cost of gadolinium.

- **Chapter I:** This chapter will provide a comprehensive scientific overview of the perovskite structure. It will start with a general description of the structure, followed by an examination of the conditions required for its stability and various methods for its synthesis. Furthermore, the chapter will explore the physical properties of perovskite and explore potential applications associated with this structure.
- **Chapter II:** The second chapter is a review of the methods and materials that were used in this work, starting with the used raw materials in the preparation method to the deferent types of analysis that have been done, the sample making, and ending with the used equipment.

- **Chapter III:** The third chapter is mainly a discussion to the $La_{(1-x)}Mg_xMnO_3$ composites analysis results which consists of :

  - ✓ A thermal study to the behavior of $La_{0.7}Mg_{0.3}MnO_3$ using TG/DTG and DSC.
  - ✓ Analysis by XRD for $La_{0.7}Mg_{0.3}MnO_3$.
  - ✓ The calculation of activation energy E_a and Avrami coefficients m, n and the oscillation coefficient k_0 in integral isoconversional methods and differential isoconversional methods.
  - ✓ Qualitative analysis of $La_{(1-x)}Mg_xMnO_3$ in terms of treatment temperature .
  - ✓ The calculation of crystal size (from the XRD data) and Tolerance Factor.
  - ✓ The calculation of the expansion coefficient is performed using two methods: firstly, by utilizing dilatometric equipment, and secondly, through local analysis using in situ XRD (HTK-XRD).

Chapter 1

Bibliographic Study of Perovskite-Type Oxides

I.1. Introduction

Perovskite structures, named after the Russian mineralogist Perovski , are one of the most fascinating structures found in nature. Their basic chemical formula is ABX_3, where A and B are metallic cations and X is typically an anion, most commonly oxygen. The packing of these anions is compact and creates spaces or "interstices" for the larger A and smaller B cations. In terms of their valency, the A cation can be mono-, di-, or trivalent, while the B cation can be divalent, trivalent, tetravalent, or pentavalent. This range of valencies allows for a vast array of combinations and possible substitutions, either partial or total. This results in an immense number of potential compounds that can be derived from the base Perovskite structure. Furthermore, the physical and chemical properties of these compounds are heavily influenced by a multitude of factors.

These factors include the type and oxidation states of the cations, the stoichiometry of the anionic and cationic elements, the precise configuration of the crystalline structure, and the techniques used in the compound's synthesis and processing.

$LaMnO_3$ perovskite is the foundational compound for a range of manganese-based materials, following the general formula $A_{1-x}B_xMnO_3$. When doped with alkaline-earth cations, these materials showcase exceptionally large variations in electric and thermal conductivity when exposed to external magnetic fields. This notable effect, coined as "colossal magnetoresistance," was first discovered in 1994 by Jin and his team. However, the exact cause of this potentially beneficial property remains largely unknown, and while doping plays a crucial role, its specific function is not entirely understood. What is well established is that these oxides' significant magnetoresistance is linked to a unique metal-insulator transition involving a complex interaction of magnetic, charge, and orbital degrees of freedom. The understanding of these metal-insulator transitions requires a deep knowledge of the electronic structure of the parent compound material. Groundbreaking neutron diffraction research by Wollan and Koehler demonstrated that undoped $LaMnO_3$ behaves as an A-type antiferromagnetic (AAF) insulator, with antiferromagnetic coupling in the b direction and ferromagnetic coupling in the ac planes.

Doping this material alters its magnetic ordering, which can result in a ferromagnetic cell or several types of antiferromagnetic cells, depending on the degree of doping. Alongside this, and again contingent on the amount of doping, the compound can exhibit a mixed valence character. The combination of these attributes, together with the variety of possible metal-

insulator transitions, leads to a rich and exceedingly complex phase diagram for this class of materials.

Overall, the Perovskite structure presents an extraordinarily versatile framework in the world of materials science and chemistry due to its flexible nature and the vast range of compounds it can generate.

I.2. The Perovskite Structure

One of the most impressive structures ever is the perovskite structure. Perovski, a Russian mineralogist, made the discovery of calcium titanate ($CaTiO_3$) in 1839, which is regarded as the discovery that gave rise to perovskite. Materials with the same type of crystal structure as $CaTiO_3$ are known as perovskite materials [1]. Perovskite materials are generally described by the chemical formula ABX_3 [2].

The ABO_3 perovskite structure can have various cations occupying its A and B sites. The A site can be occupied by monovalent cations such as M^{+1} (e.g., Na, K, ..), divalent cations such as M^{2+} (e.g., Ca, Sr, Ba,), or trivalent cations such as M^{3+} (e.g., La, Fe). On the other hand, the B site can be occupied by pentavalent cations such as M^{5+} (e.g., Nb, W), tetravalent cations such as M^{4+} (e.g., Ce, Ti), or trivalent cations such as M^{3+} (e.g., Mn, Fe) [3]. For the formation of the perovskite structure, the sum of the valence numbers of the binary compounds(A^{+m},B^{+n}) must be equal to +6 for the overall charge to be neutral [4].

In addition to insulators (like the majority of perovskites, which have high electrical resistivities), the materials also include semiconductors, superconductors, and ionic conductors [3]. The ions occupying lattice sites A and B are detailed in Figure I. 1 [5].

The ideal cubic perovskite structure is shown in Figure I. 2, where the A cations are shown at the corners of the cube, and the B cation in the centre with oxygen anions in face-centered positions. Cubic perovskites have the space group $Pm\bar{3}m$, and the equivalent positions of the atoms are detailed in Table I. 1 [6].

Table I. 1: Atoms positions on cubic perovskites [8].

A at the origin	B at the origin
$\boldsymbol{A(0,0,0)}$	$\boldsymbol{B(0,0,0)}$
$\boldsymbol{B\left(\frac{1}{2},\frac{1}{2},\frac{1}{2}\right)}$	$\boldsymbol{A\left(\frac{1}{2},\frac{1}{2},\frac{1}{2}\right)}$
$\boldsymbol{O_1\left(0,\frac{1}{2},\frac{1}{2}\right)}$	$\boldsymbol{O_1\left(\frac{1}{2},0,0\right)}$
$\boldsymbol{O_2\left(\frac{1}{2},0,\frac{1}{2}\right)}$	$\boldsymbol{O_2\left(0,\frac{1}{2},0\right)}$
$\boldsymbol{O_3\left(\frac{1}{2},\frac{1}{2},0\right)}$	$\boldsymbol{O_3\left(0,0,\frac{1}{2}\right)}$

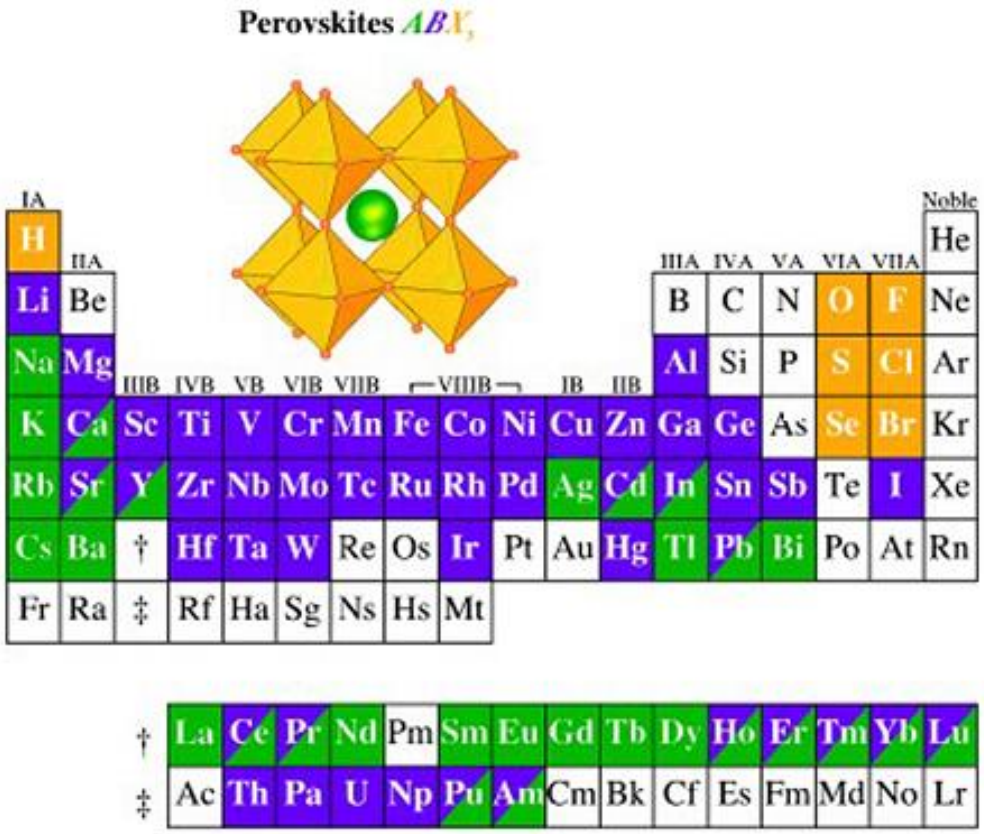

Figure I.1 : Periodic table showing the elements occupying the cationic positions of site A, B and the anion positions of site X in the perovskite structure [5].

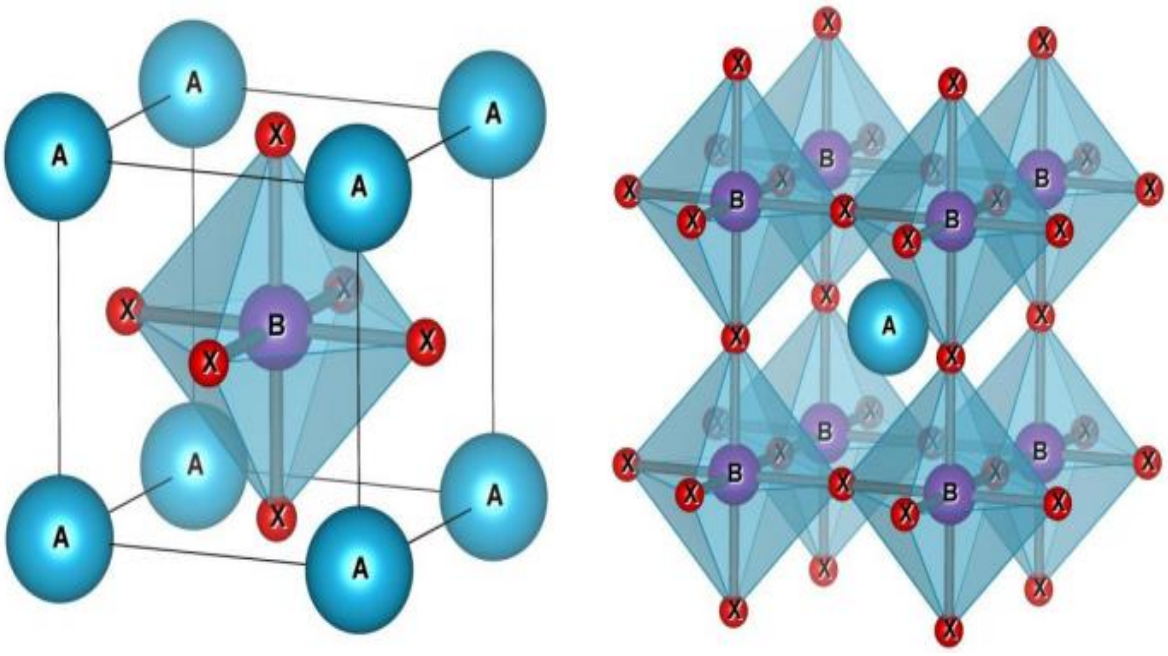

(a) (b)

Figure I.2: ABX_3 perovskite structure cubic, (a) B at the origin, (b) A at the origin [7].

I.3. Types of Perovskite

There are generally two types of perovskites (Simple and Complex perovskite structure) following the occupation of the A and B sites [9]:

Simple perovskite structure

In this case, The A and B cations are occupied with one type of atom ($BaTiO_3$, $PbTiO_3$, $CaTiO_3$ ….)

Complex perovskite structure

In this type from the structural composition, A or B are occupied with two types of atoms: $PbSc_{0.5}Ta_{0.5}O_3$, $Na_{0.5}Bi_{0.5}TiO_3$,…

I.4. Conditions for The Stability of Perovskite Structure

The stability of the perovskite structure relies on three necessary factors: the tolerance factor, the Jahn-Teller effect, and the Glazer classification, which will each be discussed one by one in the following section

I.4.1. Tolerance Factor

The tolerance factor (or Goldschmidt factor), denoted as τ, is an important stability criterion of the perovskite structure. This factor can be calculated as shown in figure I.3 using the following formula [10]:

$$\tau = \frac{(R_A + R_X)}{\sqrt{2}(R_B + R_X)} \qquad \text{I.1}$$

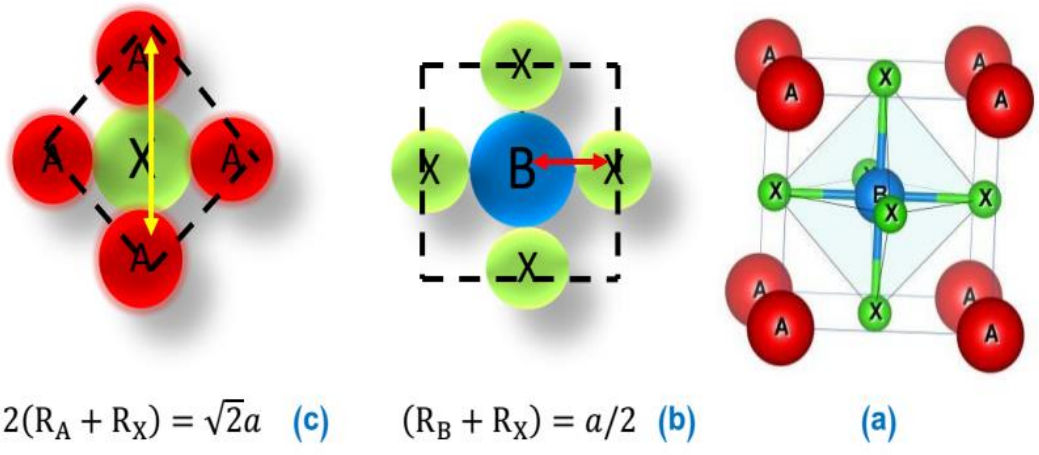

Figure I.3: Calculation of the Goldschmidt Tolerance Factor for a Cubic ABX_3

R_A, R_B, and R_X are the radii of cations A and B and anion X, respectively. The symmetry changes depending on the value of τ, as shown in the Table I.2

Table I.2 : Distortions of perovskite structure according to the values of t[11] **.**

<table>
<tr><td rowspan="2">t<0.75
ilmenite</td><td colspan="3">0.75<t<1.06
perovskite</td><td rowspan="2">t>1.06
hexagonal</td></tr>
<tr><td>0.75<t<0.95
orthorhombic distortion</td><td>0.96<t<0.99
rhomboedric distortion</td><td>0.99<t<1.06
cubic</td></tr>
</table>

1.4.2. Jahn-Teller Effect

The Jahn-Teller effect, named after Hermann Arthur Jahn and Edward Teller, is a geometric distortion of molecules and ions that is associated with certain electron configurations. This distortion leads to a lower overall system energy, and thereby stabilizes the molecule or ion. It is particularly observed in octahedral coordination compounds and in certain types of perovskite ABO_3 materials. In ABO_3 perovskite structures, the B cation is typically six-fold coordinated with oxygen, creating an octahedral geometry. If the B cation is a transition metal with a degenerate (equal energy) electron configuration, the Jahn-Teller effect can come into play.

The Jahn-Teller theorem states that any non-linear molecule with a spatially degenerate electronic ground state will undergo a geometrical distortion that removes that degeneracy, because the distorted molecule has a lower total energy than the undistorted molecule. The distortion typically involves elongation or compression of the bond lengths, or a change in the bond angles, resulting in a distortion of the BO_6 octahedra in perovskite materials.

in perovskite materials like $LaMnO_3$, where Mn is in a 3+ state (Mn^{3+}), the high-spin d electron configuration is degenerate. According to the Jahn-Teller theorem, this degenerate state will cause the MnO_6 octahedra to distort, resulting in an elongation or compression of the Mn-O bond lengths. This distortion can significantly affect the physical properties of the perovskite, such as its electronic, magnetic, and optical properties.

The Jahn-Teller effect can also cause a splitting of the energy levels in the d orbitals of the B cation, which can affect the way the material absorbs and emits light. This is particularly important in perovskite materials used in photovoltaic and light-emitting applications. Overall, understanding the Jahn-Teller effect is critical in tuning and predicting the properties of ABO_3 perovskite materials, and thereby optimizing their performance in various applications.

The deformation of crystal structure can be caused by elongation or compression in the octahedrons BO_6, and this effect is known as the Teller-Jahn effect. The B cations are located in the center of the oxygen octahedron with a d3 upper electronic layer, as This layer has five orbitals (d_z^2,$d_{x^2-y^2}$,d_{xy},d_{yz},d_{xz}). In addition, these five atomic orbitals can subdivide into the T_{2g} and Eg energy levels. While T_{2g} consists of three orbitals, E_g consists of two orbitals. Additionally, the energy generated by the T_{2g} orbitals is lower than the energy provided by the E_g orbitals.

The Teller-Jahn effect leads to a degenerate state of energy levels in T_{2g} and E_g orbitals. This effect exists in specific electronic configurations depending on number of electrons and the spin orientation (up or down). This effect states, "For the asymmetrical occupation of orbitals in non-linear, the molecule must be distorted to reduce the symmetry and energy in the system." And this is done based on the electrons in the d3 layer of B cations. In addition, the levels of the T_{2g} and E_g orbitals are energy-separated decreases to stabilize the deformed structure and minimize it in the total energy of the system, as shown in figure (I.4) [12, 13]

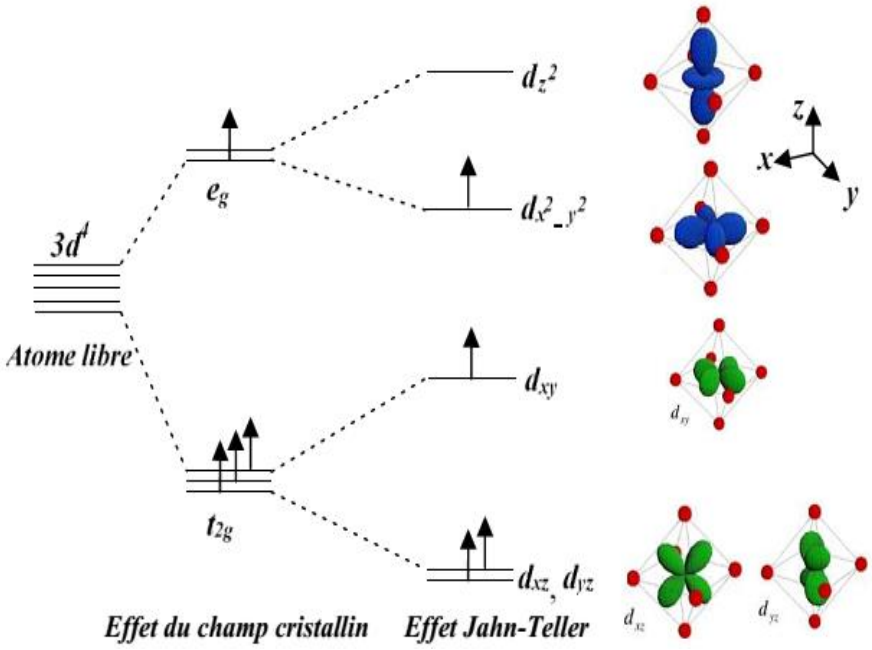

Figure I.4: The splitting of the 3d electron layer in cation B due to the Jahn-Teller effect[3].

I.4.3. Glazer Classification

The Glazer notation, named after A. M. Glazer, is a way of classifying the different types of tilts and rotations that can occur in the BO_6 octahedra in perovskite ABO_3 structures. These tilts and rotations can have a significant effect on the properties of the perovskite, including its electrical, magnetic, and optical properties.

In 1972, Glazer proposed a notation that allowed classifying all the octahedron rotations about the three axes in the perovskite structure. This notation describes 23 tilt systems that have been studied since then by Woodward as well. Tilt is explained by determining the rotation of the octahedron around the three possible axes of the ideal perovskite structure [14, 15] . The rotation around each axis is described by two symbols [16]:

- **The first symbol**

The letters a, b and c are used to denote the magnitudes of tilt about the [100], [010] and [001] pseudocubic axes sequentially .

- **The second symbol**

The second symbol indicates whether the rotation of adjacent layers is in the same direction (+) or the opposite direction (-) around the axis. The symbol 0 indicates the absence of rotation around the considered axis. Figure (I.5) is an example shows Glazer's observations for different groups

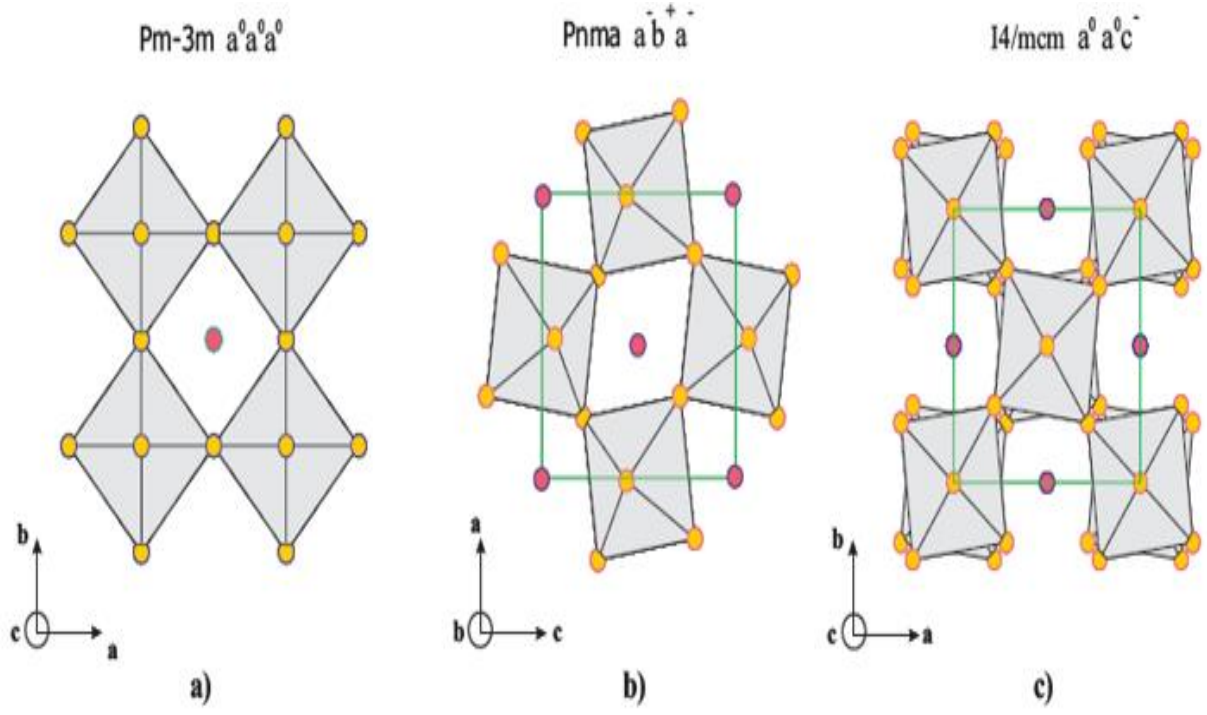

Figure I.5: Example of Glazer's observations for different groups[12].

- $\mathbf{a^0\ a^0\ a^0}$: This describes the ideal structure of the perovskite with the cubic space group Pm-3m.
- $\mathbf{a^-b^+\ a^-}$: The rotational capacity around the a and c directions are the same but different in b direction. The neighboring octahedral rotations are opposite in the a and c directions but identical in the b direction. This representation corresponds to the space group Pnma.
- $\mathbf{a^0\ a^0\ c^-}$: The rotational capacity occurs along the a and b axes (i.e. in the basal plane), but there is rotation along the c axis with opposite movement between each layer. This representation corresponds to the space group I/4 mcm[12].

The Glazer notation provides a useful tool for understanding and predicting the properties of perovskite materials based on their crystal structure. Understanding the relationship between the tilt system and the properties of the perovskite can help in the design and optimization of perovskite materials for specific applications.

I.5. $LaMnO_3$ Compound

Lanthanum manganite is an inorganic compound with the chemical formula $LaMnO_3$, often abbreviated as LMO. It is formed in the perovskite structure, consisting of an oxygen octahedral with a central Mn atom shown in figure I-6 [17]. So far, $LaMnO_3$ has been proven to possess peculiar electrical and catalytic properties in the sensor field [18]. It has been demonstrated that those properties strongly depend on the preparation method[19].

Lanthanum manganite contains La and Mn in the +3 oxidation state. When some La atoms are replaced with divalent atoms like Mg or Ba, an equivalent amount of tetravalent Mn^{+4} atoms is introduced. Such substitution, or doping can induce various electronic effects,which form the basis of a rich and complex electron correlation phenomena that yield diverse electronic phase diagrams in these alloys. These effects form the foundation of a complex electron correlation phenomenon that yields a rich and diverse set of outcomes.[20].

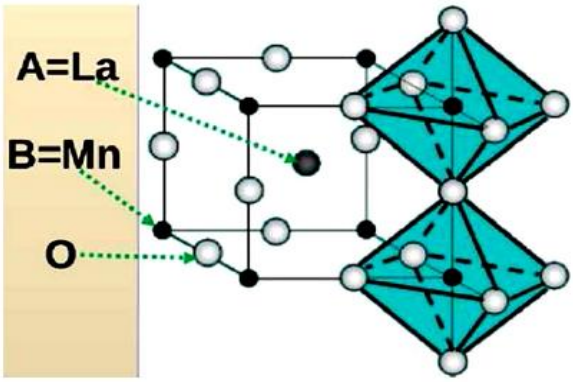

Figure I. 6: Ideal cubic perovskite $LaMnO_3$ [21].

I.6. Property of $LaMnO_3$

$LaMnO_3$, or Lanthanum Manganite, exhibits numerous interesting properties due to its perovskite structure and the interplay of the atoms within that structure. Here are some of the significant properties:

- Magnetic Properties: $LaMnO_3$ shows antiferromagnetic ordering below a certain temperature known as the Néel temperature, typically around 140 K. Antiferromagnetism is a phenomenon in which the magnetic moments of atoms or ions in a crystal lattice align in a regular pattern with neighboring spins pointing in opposite directions, resulting in zero net magnetization. This behavior results from superexchange interactions between Mn^{3+} ions mediated by oxygen.
- Jahn-Teller Distortion: The Mn^{3+} ion in $LaMnO_3$ is subject to a strong Jahn-Teller effect, a geometric distortion of the MnO_6 octahedra that lifts the degeneracy of energy states in the system, reducing its overall energy. The Jahn-Teller distortion in $LaMnO_3$ is responsible for its antiferromagnetic properties and contributes to the observed electronic and structural properties of the material.
- Colossal Magnetoresistance (CMR): Although pure $LaMnO_3$ does not exhibit CMR, doping it with divalent ions like Sr^{2+} to form $La_{1-x}Sr_xMnO_3$ creates mixed-valence manganites that can show this effect. CMR is a dramatic change in electrical resistance in the presence of a magnetic field. It's a phenomenon with potential applications in magnetic field sensors and data storage technology.
- Dielectric and Ferroelectric Properties: $LaMnO_3$ can also exhibit strong dielectric behavior and show signs of ferroelectricity under certain conditions. This means it can polarize in response to an electric field and retain this polarization even after the field is removed. These properties make it potentially useful in capacitors and other electronic components.
- Thermal and Chemical Stability: $LaMnO_3$ is stable over a wide range of temperatures and resistant to many chemical reactions, making it durable for use in various environmental conditions.
- Optical Properties: The band gap (energy difference between the valence band and conduction band) of $LaMnO_3$ is in the visible light region. Therefore, this material also shows potential for use in optoelectronic devices.

The ability to adjust these properties by doping $LaMnO_3$ with various elements makes it a fascinating compound for research in solid-state physics, materials science, and various

technological applications. However, while there has been substantial research on $LaMnO_3$, the exact mechanisms underlying some of its properties, such as CMR, are complex and not fully understood, remaining an active area of study.

I.6.1 Property of $LaMnO_3$ at High Temperature

$LaMnO_3$ is a perovskite-structured compound that displays interesting physical properties due to the interactions between the spin, charge, and lattice degrees of freedom in the Mn3+ ions. Some properties of $LaMnO_3$ at high temperatures include [17]:

- **Structural Changes**: At high temperatures, structural changes may occur in LaMnO3. At room temperature, $LaMnO_3$ adopts an orthorhombic perovskite structure. However, above certain temperatures (usually above 800°C), it can potentially transform to a more symmetrical.
- **Electrical Conductivity**: At room temperature, LaMnO3 behaves as an insulator, but it can become a conductor at high temperatures. This transition is usually due to thermal excitation of electrons to the conduction band.
- **Magnetic Properties**: $LaMnO_3$ is a type of compound known as an insulator. It demonstrates an interesting magnetic behavior called antiferromagnetism at low temperatures, but this can change with increasing temperature. At high temperatures, thermal agitation can cause a transition to a paramagnetic state.
- **Thermal Expansion**: Like other materials, $LaMnO_3$ typically expands as it is heated. This is due to the thermal agitation of the atoms, which increases the average separation between them.
- **Ionic Conductivity**: High-temperature can potentially enhance the ionic conductivity of $LaMnO_3$. This is typically the case for oxide materials, as vacancies in the crystal lattice (usually oxygen vacancies) become mobile at high temperatures, leading to ionic conduction.

However, please note that the exact changes in the properties of $LaMnO_3$ will depend on the specific conditions, including the precise temperature and the surrounding environment.

I.6.2 Property of $LaMnO_3$ at Low Temperature

At low temperatures, $LaMnO_3$ primarily behaves as an antiferromagnetic insulator, exhibiting an orientation of neighboring manganese atomic spins in opposite directions, thereby resulting in a net magnetization of zero.

Additionally, this antiferromagnetic behavior is typically accompanied by a Jahn-Teller distortion a- minor lattice distortion that results from the elongation or compression of the MnO_6 octahedra within the perovskite structure. This distortion is supposed to be intimately connected with the hybridization between Mn 3d and O 2p orbitals, significantly influencing the magnetic and electronic properties of $LaMnO_3$.

In its low-temperature state, $LaMnO_3$ also exhibits "orbital ordering," a phenomenon in which the electronic orbitals of the manganese ions arrange themselves in a periodic pattern. This ordering is closely associated with both the Jahn-Teller distortion and the antiferromagnetic ordering, demonstrating the interplay between the lattice, charge, spin, and orbital degrees of liberty in $LaMnO_3$.

Furthermore, the electronic and magnetic properties of $LaMnO_3$ can be dramatically manipulated through doping or application of external pressures. This can introduce a boost of intriguing phenomena such as colossal magnetoresistance, charge ordering, and even multiferroic behavior, all of which offer a rich playground for the exploration of correlated electron physics and potential technological applications.

It is evident that $LaMnO_3$ serves as an archetype of a class of complex oxides where interplay among multiple degrees of liberty leads to a wide array of physical phenomena. These characteristics, coupled with the potential for manipulating them for technological uses, make $LaMnO_3$ an attractive topic of research in the field of materials science [17].

I.7. Effects of Mg Doping on $LaMnO_3$

Mg is an alkaline earth element that can replace both La and Mn sites in $LaMnO_3$, studies have shown that Mg substitution at the A-site of $LaMnO_3$ can enhance the formation of Mn4+ ions, leading to improved catalytic activity in the combustion of volatile organic compounds . However, Mg substitution at the A-site of $LaMnO_3$ can cause the total charge imbalance of B-site, which significantly improves the amount and reactivity of surface active oxygen species. in addition, MgO has been proven to improve the thermal stability , pores structure and NO adsorption and activation ability of catalysts[22, 23].

I.8. Perovskites: Synthesis and Processing Methods

synthesis of perovskite materials, a variety of approaches have been employed, including solid-state reaction from oxides, solegel, hydrothermal synthesis, high-pressure synthesis, and mechanically-activated synthesis, among others. This research acknowledges the complexity of such processes, as different procedures may yield compounds with identical chemical compositions yet display significant variations in crystalline symmetry and structure.

I.8.1 Solid-State Method

Solid-state reactions involve mixing raw materials and final products in a solid-state, allowing nitrates, carbonates, oxides, and other substances to be combined in stoichiometric ratios. Perovskites can be synthesized through solid-state reactions by mixing carbonates or oxides of A- and B-site metal ions in the appropriate proportions to achieve the desired composition of the perovskite formula ABO_3 [24, 25]. They are ball milling effectively in an appropriate milling media of acetone or isopropanol .Then the obtained product is dried at 100 °C and calcined in air at 600 °C for 4–8 h under heating/cooling rates of 2 °C/min. After that, the calcined samples are ground well and sieved. Then it was calcined again at 1300–1600 °C for 5–15 h under the heating/cooling rate of 2 °C/min to confirm the formation of single phase of perovskite. Again grinding and sieving was carried out for the calcined samples[26].

I.8.2 Sol-Gel Method

The sol-gel technique allows for the production of materials through simple chemical reactions carried out at temperatures close to room temperature [27]. This method has the advantage of being fast and producing chemically pure materials with nanometric sizes.

The operating protocol for this technique consists **:**

- ✓ First of all , Dissolving the precursor materials as nitrates in distilled water using magnetic stirring on a hot plate.
- ✓ At T=70°C , Quantities of citric acid are added in order to complete the homogeneity of the solution.
- ✓ By increasing the temperature up to 180°C, the solution is slowly evaporated and a viscous gel is formed. This gel, when heated to 350°C, results in a black powder.

I.8.3 Coprecipitation Method

Coprecipitation is easy to implement and it also makes it possible to control the homogeneity of the sizes as well as the morphology of the crystallites.

This method involves coprecipitating metal chloride precursors in an aqueous phase by adding sodium hydroxide (NaOH) under high-speed agitation. The resulting synthesis suspension is then introduced into a boiling water bath and stirred for 2 hours, followed by 30 minutes of agitation. A brown precipitate obtained after rinsing and filtration is heated for 2 hours at 100°C then at 700°C. Nanoparticles are then obtained after cooling[3]. However, this technique has some drawbacks such as the loss of stoichiometry during the filtration steps due to the inevitable difference in solubility between the precipitates and generally the formation of aggregates during synthesis[28].

I.8.4 Mechanosynthesis Method

Mechanosynthesis has gained significant interest due to the growing interest in nanomaterials and metastable materials. It is defined as a process of synthesis of materials by dry grinding in a high energy[29].

The elaboration by mechanosynthesis consists of mixing, by grinding, micrometric powders (1 to 50 µm) of several alloys. The powders are introduced into a jar containing steel or tungsten balls. The whole is vigorously agitated, allowing for plastic deformation accompanied by high-energy mechanical wear. Phase transitions under mechanical shock lead to the formation of compounds defined (intermetallic) but also make it possible to develop supersaturated crystalline solid solutions, high temperature crystalline phases, nano composites , It should also be remembered the strong potential of this technique in the synthesis of amorphous materials[3].

I.9. Perovskite Materials Properties and Applications

In recent years, perovskite materials are becoming more interesting and important due to their great potential for contributing to solid oxide fuel cells, solid electrolyte, fixed resistance, electromechanical devices, transistors, etc…, due to the particular crystalline structure, magnetism, electrical conductivity, piezoelectric and electro-optical properties, catalytic activity and gas sensitivity,…etc as shown in Table I.3 [30].

I.9.1. Electrical Properties

Perovskites play an important role in modern electronics. They are used in memory devices, capacitors, microwave devices, pressure gauges, and ultra-fast electronics such as maglev trains.[31]

They are superconducting at relatively high temperatures, transform mechanical pressure or heat into electricity (piezoelectricity), accelerate chemical reactions (catalysts), and suddenly change their electrical resistance when placed in a magnetic field (magnetoresistance). Many electrochemical studies on electrodes based on these oxides have been conducted in aqueous environments. They have revealed an important electrocatalytic role in the oxygen electrode reaction at room temperature[32] .

These highly promising materials are increasingly finding applications in transparent ceramics, photovoltaic cells, and fuel cells. Perovskites have nearly universal possibilities for use because it is possible to vary their properties within very wide limits. They are also known as chemical chameleons for this reason. [33].

I.9.2. Physical Properties

I.9.2.1. Ferroelectricity

Ferroelectric crystals exhibit a spontaneous polarization of charge that can be controlled by an external electric field. In addition to other perovskites, $BaTiO_3$, $LiNbO_3$, and $KNbO_3$ all exhibit spontaneous polarization.

I.9.2.2. Piezoelectricity

Piezoelectricity is the property of certain materials to become electrically polarized under the action of a mechanical force (direct effect) and reciprocally to deform when an electric field is applied to them (inverse effect). Piezoelectric materials are very numerous, the most well-known piezoelectric material is quartz, which is used in watches to produce clock pulses[34].

I.9.2.3. Magnetoresistance

Perovskites suddenly change their electrical resistance when placed in a magnetic field. They are used in magnetic tapes and discs [35].

I.9.2.4. Superconductivity

Perovskites are superconductors at high temperatures. They are used in capacitors, microwave devices and high-speed electronics[35].

Table I.3 : Physical properties of certain compounds with perovskite-type structure[36].

Composition	**physical property**	**application**
$CaTiO_3$	Dielectricity	Microwave
$BaTiO_3$	Ferroelectricity	Non-volatile computer memories
$PbZr_{1-x}TixO_3$	Piezoelectricity	Probes
$Ba_{1-x}La_xTi_xO_3$	Semiconductor	Semiconductor
$Y_{0.33}Ba_{0.67}CuO_{3-\alpha}$	Superconductor	Magnetic Signal Detectors
$(Ln ,Sr)CoO_{3-\alpha}$	Mixed conductors	Gas diffusion membranes
$BaInO_{2.5}$	Ion conductor	Electrolyte in fuel cells
$AMnO_{3-\alpha}$	Giant magnetoresistance	Read heads for hard disks

I.10. References

1. Varma, P. R. (2018). Low-dimensional perovskites. In Perovskite Photovoltaics (pp. 197-229). Academic Press.
2. Moure, C., & Peña, O. (2015). Recent advances in perovskites: Processing and properties. Progress in Solid State Chemistry, 43(4), 123-148.
3. Dhahri, A. (2022). Etude des propriétés magnétiques et diélectriques des oxydes de fer et leurs applications (Doctoral dissertation, 00500:: Universidade de Coimbra).
4. Etchegoyen, G. (2005). Développement d'une membrane céramique conductrice mixte pour la production de gaz de synthèse (Doctoral dissertation, Limoges).
5. Petrović, M., Chellappan, V., & Ramakrishna, S. (2015). Perovskites: solar cells & engineering applications–materials and device developments. Solar Energy, 122, 678-699.
6. Levy, M. R. (2005). Crystal structure and defect property predictions in ceramic materials (Doctoral dissertation, University of London).
7. Souidi, A. Etude des propriétés spintroniques du double Perovskite type $ABCO_6$ (Doctoral dissertation, Université de Mostaganem-Abdelhamid Ibn Badis).
8. Boudali, A. (2011). Etude des propriétes structurales, Elastiques, Electroniques et Optiques des perovskites cubiques $LaA1O_3$ et $XTiO_3$ (X= Ca, Sr, Pb) (Doctoral dissertation, Université d'Oran1-Ahmed Ben Bella).
9. Tedjani, S. (2016). Calculation of the oxygen rate in the Ca1-xSrxFeO2. 5+ y compounds.
10. Boualleg, C. (2020). Etude des propriétés structurales électroniques et élastiques des nouvelles pérovskites CsCaF3-yCly et CsCaCl3-yBry (y= 0, 1, 2 et 3).
11. Lamrani, N. (2011). Synthèse et caracterisation de matériaux dielectriques à structures perovskite complexe de type Ca1-xAxTi1-y bY03 (A= Sr, B= Zr,...) (Doctoral dissertation, Universite Mouloud MAMMERI Tizi-Ouzou).
12. Autret, C. (2002). Etudes de pérovskites de manganèse (et structures dérivées) à propriétés de magnétorésistance colossale (Doctoral dissertation, Caen).
13. Michel, M. R. (2010). Electronic structure study of copper-containing perovskites (Doctoral dissertation, UCL (University College London)).
14. Glazer, A. M. (1972). The classification of tilted octahedra in perovskites. Acta Crystallographica Section B: Structural Crystallography and Crystal Chemistry, 28(11), 3384-3392.

15. Woodward, P. M. (1997). Octahedral tilting in perovskites. I. Geometrical considerations. Acta Crystallographica Section B: Structural Science, 53(1), 32-43.
16. Woodward, D. I., & Reaney, I. M. (2005). Electron diffraction of tilted perovskites. Acta Crystallographica Section B: Structural Science, 61(4), 387-399.
17. Lewetegn, K. (2018). synthesis and characterization of lamno3-δ based advanced ceramic materials for solid oxide fuel cells.
18. Xu, D., Luo, L., Ding, Y., Jiang, L., Zhang, Y., Ouyang, X., & Liu, B. (2014). A novel nonenzymatic fructose sensor based on electrospun LaMnO3 fibers. Journal of Electroanalytical Chemistry, 727, 21-26.
19. Zou, G., Wang, Z., Sun, M., Luo, X., & Wang, X. (2011). A novel solid-gas process to synthesize LaMnO3 perovskite with high surface area and excellent activity for methane combustion. Journal of natural gas chemistry, 20(3), 294-298.
20. Fattah, Z. A. international journal of engineering sciences & research technology structural and transport properties of te doped lamno3.
21. Hernández, E., Sagredo, V., & Delgado, G. E. (2015). Synthesis and magnetic characterization of LaMnO3 nanoparticles. Revista mexicana de física, 61(3), 166-169.
22. Zeng, Y., Wang, Y., Zhang, S., & Zhong, Q. (2020). Partial substitution of magnesium in lanthanum manganite perovskite for nitric oxide oxidation: The effect of substitution sites. Journal of Colloid and Interface Science, 580, 49-55.
23. Zhang, C., Hua, W., Wang, C., Guo, Y., Guo, Y., Lu, G., ... & Giroir-Fendler, A. (2013). The effect of A-site substitution by Sr, Mg and Ce on the catalytic performance of LaMnO3 catalysts for the oxidation of vinyl chloride emission. Applied Catalysis B: Environmental, 134, 310-315.
24. Nieto, S., Polanco, R., & Roque-Malherbe, R. (2007). Absorption kinetics of hydrogen in nanocrystals of BaCe0. 95Yb0. 05O3-δ proton-conducting perovskite. The Journal of Physical Chemistry C, 111(6), 2809-2818.
25. Mastai, Y. (Ed.). (2012). Advances in crystallization processes. BoD–Books on Demand.
26. Atta, N. F., Galal, A., & El-Ads, E. H. (2016). Perovskite nanomaterials–synthesis, characterization, and applications. Perovskite Materials–Synthesis, Characterisation, Properties, and Applications, 107-151.

27. Gopalan, E. V., Joy, P. A., Al-Omari, I. A., Kumar, D. S., Yoshida, Y., & Anantharaman, M. R. (2009). On the structural, magnetic and electrical properties of sol–gel derived nanosized cobalt ferrite. Journal of Alloys and Compounds, 485(1-2), 711-717.
28. Thang, P. D., Rijnders, G., & Blank, D. H. (2005). Spinel cobalt ferrite by complexometric synthesis. Journal of magnetism and magnetic materials, 295(3), 251-256.
29. Sani, R., Beitollahi, A., Maksimov, Y. V., & Suzdalev, I. P. (2007). Synthesis, phase formation study and magnetic properties of $CoFe_2O_4$ nanopowder prepared by mechanical milling. Journal of materials science, 42, 2126-2131.
30. Lebid, M. (2016). Etude des propriétés physicochimiques des oxydes à base de lanthane, fer et magnésium (Doctoral dissertation, Université Mohamed Khider-Biskra).
31. OGBI Nour El Houda, M. K. caractérisation physicochimique d'un oxyde pérovskyte.
32. Salmi, S., & Benchaabane, S. (2019). Synthèse et Caractérisation physicochimiques De la pérovskite $LaFeO_3$ (Doctoral dissertation, UNIVERSITE MOHAMED BOUDIAF-M'SILA).
33. Mya, O. B. (2015). Synthèse et Caractérisation de la pérovskite La1-xSrxFe0. 7Ni0. 3O3 (Doctoral dissertation).
34. HASNI, W. (2016). Le multiferroïsme dans les pérovskites à base des terres rares: Étude de premier principe (Doctoral dissertation).
35. Rima, H. (2014). Effet de la température de calcination et de l'agent de complexation sur les propriétés structurales d'un oxyde mixte. Mémoire de Master, Université Mohamed Khider de Biskra.
36. Mahboub, M. S., & Boudjada, A. (2017). Synthèse, caractérisation par diffraction X et spectroscopie Raman des composés $Ca1\text{-}xSrxFeO_2$. 5-δ (δ= 0, 0.5).

Chapter 2

Materials and methods

II. Materials and Methods

II.1. Introduction

Sample preparation is an essential step in our work. This chapter presents the experimental protocol for preparing lanthanum manganite doped with Magnesium cations Mg^{+2} in the La sub-lattice.The various equipment used to characterize these materials. For this, we used the following technique: X-ray diffraction (XRD), X-ray diffraction with a high-temperature chambre (XRD-HTK), Thermogravimetric Analysis (TG), differential thermal analysis (DTA), and dilatometry (DIL). The various procedure used to examine the results obtained is high-score-plus with 2023 DATA to qualitative identification, Rietveld refinement, Linear reaction models: integral iso-conversional methods and differential iso-conversional methods to study the kinetics phase formation.

II.2. The Raw Materials Used

The materials utilized in our research are shown in Figure (II-1):

- The chemical compound lanthanum nitrate hexahydrate, $La(NO_3)_3 * 6H_2O$
- The chemical compound Magnesium nitrate hexahydrate $Mg(NO_3)_2*6H_2O$
- The chemical compound Manganese Nitrate tetrahydrate $Mn(NO_3)_2*4H_2O$
- The chemical compound Citric acid monohydrate $C_6H_8O_7*H_2O$

Figure (II-1): the raw materials used.

The reaction is described according to Equation (II.1) below :

$$(1\text{-}x)\ La(NO_3)_3{*}\ 6H_2O + x\ Mg(NO_3)_2{*}6H_2O + Mn(NO_3)_2{*}4H_2O \xrightarrow{+\,°C} La_{(1-x)}Mg_xMnO_3 \quad ..(II.1)$$

In our investigation of $La_{(1-x)}Mg_xMnO_3$ compound, we studied the presence of magnesium (Mg) in the lanthanum (La) sites at different doping proportions: x = 0, 0.1, 0.2, 0.3, and 0.4 as shown in **Table (II-1 and 2)**.

Table (II-1): The dopped magnesium (x) proportion in $LaMnO_3$ compound.

x	0	0.1	0.2	0.3	0.4
Chemical compound	$LaMnO_3$	$La_{0.9}Mg_{0.2}MnO_3$	$La_{0.8}Mg_{0.2}MnO_3$	$La_{0.7}Mg_{0.3}MnO_3$	$La_{0.6}Mg_{0.4}MnO_3$

Table (II-2): quantities of fundamental components for preparing 3 grams of various powders

m(g) X	**$La(NO_3)_3 6H_2O$**	**$Mg(NO_3)_2 6H_2O$**	**$Mn(NO_3)_2 4H_2O$**	**$C_6H_8O_7$**	**$La_{(1-x)}Mg_xMnO_3$**
0	5.3714	0	3.1137	5.2138	3
0.1	5.0757	0.3339	3.2686	5.4730	3
0.2	4.7470	0.7027	4.4396	5.7595	3
0.3	4.3831	1.1123	3.6297	6.0778	3
0.4	3.9765	1.5699	3.8418	6.4332	3

II.3. Experimental Method

II.3.1. Sol-Gel Method

The sol-gel technique allows for the production of materials through simple chemical reactions carried out at temperatures near to room temperature. This method has the advantages of being fast and producing chemically pure materials with nanometric sizes. The operating protocol of this technique Figure (II-2) consists **:**

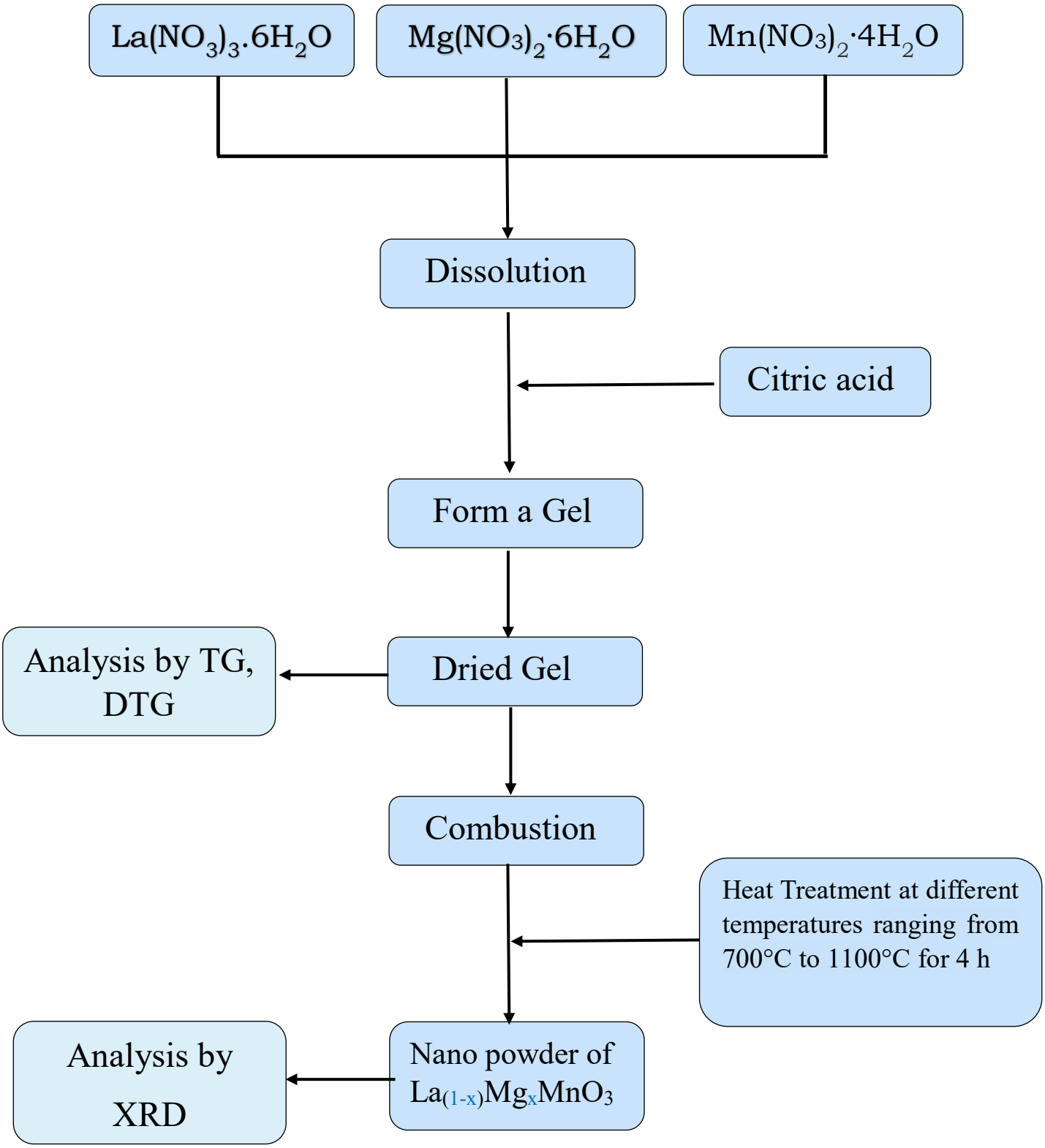

Figure (II-2): Step-by-Step Protocol for Preparing and Characterization of $La_{(1-x)}Mg_xMnO_3$ Compound.

First of all

- ✓ Measure the mass of $La(NO_3)_3$* $6H_2O$, $Mg(NO_3)_2$*$6H_2O$, $Mn(NO_3)_2$*$4H_2O$ and ($C_6H_8O_7$*H_2O).
- ✓ Dissolve $La(NO_3)_3$* $6H_2O$, $Mg(NO_3)_2$*$6H_2O$, and $Mn(NO_3)_2$*$4H_2O$ in distilled water by magnetic stirring on a hot plate.
- ✓ At T=75°C, amounts of citric acid ($C_6H_8O_7$*H_2O) are added to the solution to complete homogeneity.
- ✓ the solution is slowly evaporated and a viscous gel is formed shown in Figure (II-3).
- ✓ This gel, heated at 180°C, the citric acid decomposition and obtained black powder after this combustion shown in Figure (II-3).

The resultant powder is then subjected to a second process in which the grains are crystallized by calcination at various temperatures between 700°C and 1100°C for 4 hours Figure (II-4). After each calcining process, we manually grind the powder for a period of not less than a quarter of an hour, and the purpose is to homogenize and crush

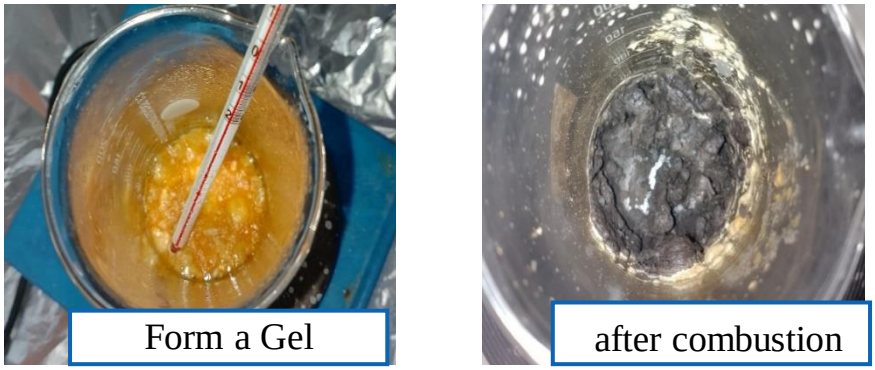

Figure (II-3): Gel formation and the powder after combustion**.**

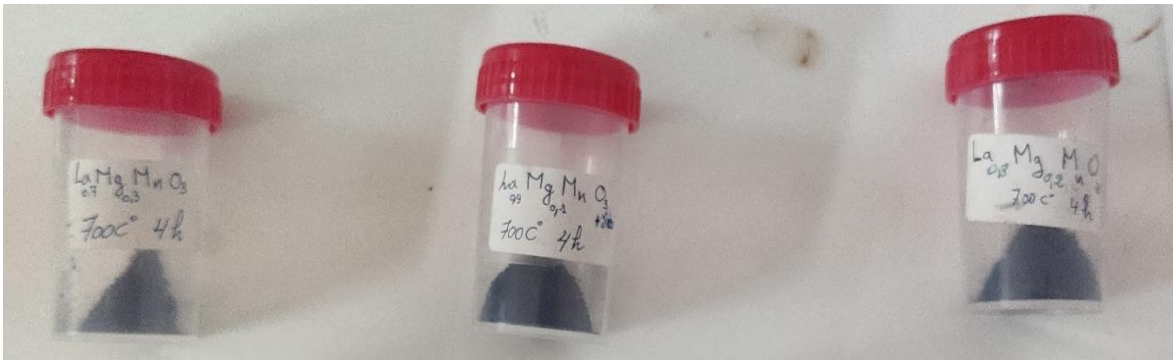

Figure (II-4): samples of $La_{(1-x)}Mg_xMnO_3$

II.4. Materials Used

II.4.1. X-Ray Diffraction (XRD)

X-ray diffraction is one of the most widely used methods in materials characterization. It enables the determination of interatomic distances and the arrangement of atoms in crystalline lattices. Since X-rays are diffracted differently by the elements of the lattice depending on their construction, irradiating a material with X-rays allows for the identification of its crystallographic nature. Furthermore, X-ray diffraction provides access to physical information about crystals, including their size and orientation. It encompasses various principles and techniques

In our analytical study, we used X-ray analysis devices for both powder preparation and the analysis of prepared samples before and after any treatment. We utilized two types of analysis instruments: the first device is available in our laboratory at the University of M'sila, and it operates at room temperature. The second device, it is located at the Nuclear Research Center in Birine, djelfa, and it is equipped with a high-temperature chamber. We used it to determine the crystal structure, lattice constants, and linear expansion coefficient.

Operating conditions

The instrument shown in Figure (II-5) is called a PANalytical X'Pert Pro, K-Alpha1 wavelength 1.5405980, Generator voltage 40 kV, Tube current 30 mA, Scan range 10 to 80°, Scan step size 0.02° and Time per step,0.50 s. used to analyze the structure of crystalline phases present within a sample are determined and the crystalline dimensions are measured using several software applications. This process involves directing a monochromatic beam of radiation onto the material and analyzing the resultant scattering pattern.

Identifying phases

The determination of phases using X-ray diffraction involves analyzing the pattern produced when X-rays interact with a material's crystal lattice. This pattern, known as the diffraction pattern, contains information about the arrangement of atoms within the crystal. By measuring the angles and intensities of the diffracted X-rays, one can identify the phases present in the material.

To accomplish this, the diffraction pattern is compared to a database of known patterns, such as the "ASTM Data Sheets." These databases contain information about the diffraction

patterns of various crystalline phases. By matching the observed pattern with the patterns in the database, the phases in the material can be determined.

The diffraction pattern provides valuable information about the interatomic distances and crystal symmetry of the material. By analyzing the positions of the diffraction peaks and their intensities, it is possible to calculate the lattice parameters and infer the crystal structure of the material.

The diffraction angles are identified by analyzing the beam on the detector in accordance according to Bragg's law.

$$2d_{hkl} \sin\theta = n \lambda$$

n: the order of reflection.

λ: wavelength of the incident wave (λ_{Cu}).

d: the inter-planner distance.

θ: the angle at which X-rays of wavelength are reflected.

II.4.2. Determination of Average Crystallite Size by Scherrer's Method

The use of X-ray diffraction (XRD) to determine the average crystallite size is a common method, based on the principle of X-ray reflection by crystalline structures. The most commonly used method to estimate crystallite size from XRD data is by employing the Scherrer formula.

The Scherrer formula is given by:

$$D = K\lambda / (\beta \cos(\theta))$$

where:

- D is the crystallite size.
- K is a dimensionless shape factor, with a value close to unity. The exact value depends on the crystallite shape.
- λ is the X-ray wavelength.

- β is the line broadening at half the maximum intensity (FWHM), after subtracting the instrumental line broadening, in radians. This quantity is inversely proportional to the crystallite size.
- θ is the Bragg angle.

This method provides an average crystallite size and assumes that the crystallites are isotropic and have a similar size distribution. However, it's important to note that this method relies on several assumptions, such as that the crystallites are homogeneous and similar in size, which may not always be the case. In cases of significant size heterogeneity, it might be more appropriate to use other techniques, such as Transmission Electron Microscopy (TEM) or Scanning Electron Microscopy (SEM).

It's worth noting that the XRD method is usually quicker and easier to use than TEM or SEM, which require more complex sample preparation and more time to collect the data. However, the latter techniques may provide more detailed information about the crystallites, including their shape and size distribution, which can be useful in certain applications.

Figure (II-5): PANalytical X'Pert Pro

II.4.3. Thermogravimetric (TG) and Differential Thermal Analysis (DTA)

The thermobalance used in our experiments (LABSYS EVO DTA/DSC-TG SETARAM instrument) enables simultaneous recording of mass variations (thermogravimetric analysis, TGA) and temperature fluctuations (differential thermal analysis, DTA). The curves derived from the TGA signal are calculated from raw measurements of mass variation.

For the procedure, we place samples in a cylindrical alumina crucible with a diameter of 4 mm and a length of 8 mm. For DTA measurements, an identical but empty crucible is used as a reference and placed on the same scale., such as thermal treatment atmosphere and degradation products. This setup only allows for the measurement of the TGA signal. the mass ranges of powder samples (contained in the crucible) from 20 to 50 mg.

We conduct tests under air, up to 1,600°C, with heating rates ranging from 0.1 to 1 °C/min.

TGA: Thermogravimetric Analysis is a method that measures the change in mass of a sample as it undergoes temperature scanning in a controlled atmosphere. This change in mass can either be a loss of mass (vapor emission) or a gain of mass (gas fixation).

DTA: differential thermal analysis is a technique measuring the difference in temperature between a sample and a reference (a thermally inert material) as a function of the time or the temperature when they undergo temperature scanning in a controlled atmosphere, this method enables any transformation to be detected all the categories of materials.

DSC: differential scanning calorimetry is a technique determining the variation in the heat flow given ou or taken in b a sample when it undergoes temperature scanning in a controlled atmosphere, with heating or cooling any transformation taking place in a material is accompanied by theexchange of heat, DSC enables the temperature of this transformation to be determined and the heat from it to be quantified.

Chapter 3

Results and Discussion

III.1 Introduction

This chapter focuses on studying various aspects related to the compound La(1-x)MgxMnO3. Differential Thermal Analysis is used to investigate phase transformations occurring in the prepared powder. X-ray equipment is employed to examine the impact of calcination temperature on the crystal structure of the compound. The relationship between crystal size, temperature, and concentration (x) of the additive is studied. Additionally, in situ XRD is utilized to observe phase transformations of the $La_{0.7}Mg_{0.3}Mn_{O3}$ powder. The mechanism of crystallization for the $La_{0.7}Mg_{0.3}MnO_3$ compound is explored using Differential Thermal Analysis. Finally, the coefficient of linear expansion is investigated by analyzing the results obtained from in situ XRD and dilatometry experiments.

III.2 Thermal Study

In Differential Thermal Analysis (DTA), the material under study and an inert reference material are heated (or cooled) simultaneously, under the same conditions. The difference in temperature between the sample and the reference is recorded as a function of temperature or time. The resulting DTA curve can show exothermic (heat-releasing) or endothermic (heat-absorbing) processes occurring in the sample, as these would cause a temperature difference between the sample and the reference.

DTA can be used to detect *Phase Transitions:* DTA helps to identify phase transitions in ceramics, such as the glass transition temperature, crystallization temperature, melting point, and more. Understanding these phase transitions is critical for predicting how ceramics will behave under different conditions. And It is used to study chemical reactions like oxidation or reduction that may occur during the firing process. This is particularly important when ceramics are used in environments where they may be exposed to extreme temperatures or corrosive elements.

Thermogravimetric Analysis (TG) measures, changes in the weight of a sample as it is heated in a controlled atmosphere. Weight loss or gain can provide valuable information about the thermal stability of the material, the nature of decomposition reactions, and the percentage of organic, inorganic, and volatile components.

III.2.1 Thermogravimetric/Differential Thermal Analysis study

Figure (III-1) shows the curves of the thermogravimetric/difference thermogravimetric analysis/differential thermogravimetric analysis (TG/DTG-DTA) of the powder-gel

composite of $La_{0.7}Mg_{0.3}MnO_3$ prepared and heated from room temperature to 600°C with a heating rate of 1°C/min. For all differential thermal analysis or mass Thermogravimetric Analysis experiments, we used the same amount of powder (50 mg)..

- Four steps of mass losses are observed in the TG curve. The first step is the dissociation of the water in citric acid and the evaporation of adsorbed water is according to the first mass loss (Δm = 14.38%). This process corresponds to the endothermic peak at 93.66 °C and 134.78 °C as seen in the DTA curve as well as the first and second peaks at 87.25°C and 120.17°C as seen in the DTG curve.
- The second step, which has a mass loss of 30.85 %, is due to the decomposition of citric acid and water contained in nitrate, which in the DTG curve at 217.85°C.
- In the third step, nitrate decomposition occurs when the mass loss equals 4.29%.
- In the last step, Δm = 1.96 %, this mass loss is due to the decomposition of the remaining nitrate.

As for the differential thermal analysis curve, a series of endothermic and exothermic transformations that occur to the powder during its thermal treatment are observed in Figure (III-1) (b):

- The first endothermic transformation is due to the evaporation of adsorbed water, which has a maximum temperature of 93.66 °C.
- A second endothermic transformation occurs in the thermal range of 117.90 to 145 °C, resulting from the exit of water entering the formation of citric acid as determined by the following equation:

$$C_6H_8O_7{*}H_2O \longrightarrow C_6H_8O_7 + H_2O$$

There are two exothermic transformations in the thermal range of 175 to 265°C, the decomposition of citric acid and water contained in nitrate. Its maximum temperature is 198°C.

- The second exothermic transformation, which has a maximum temperature of 239 °C, occurs in the thermal range between 218 to 250 °C, producing dissociation of certain metal nitrates (not all of them). The remaining material breaks down between 260 and 308 °C.
- The last exothermic transformation in the thermal range from 314 to 410 °C is caused by the formation of a crystalline phase called perovskite "$La_{0.7}Mg_{0.3}MnO_3$"; the rate of this transformation is maximum at 362.5 °C.

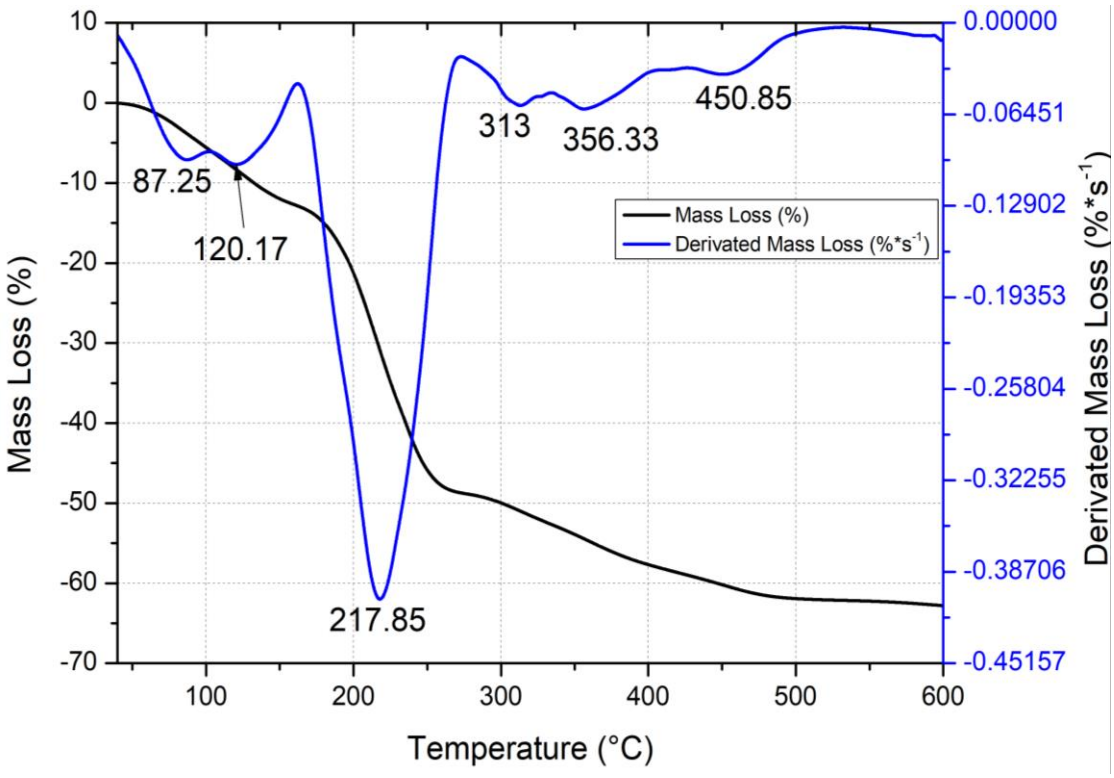

(a)

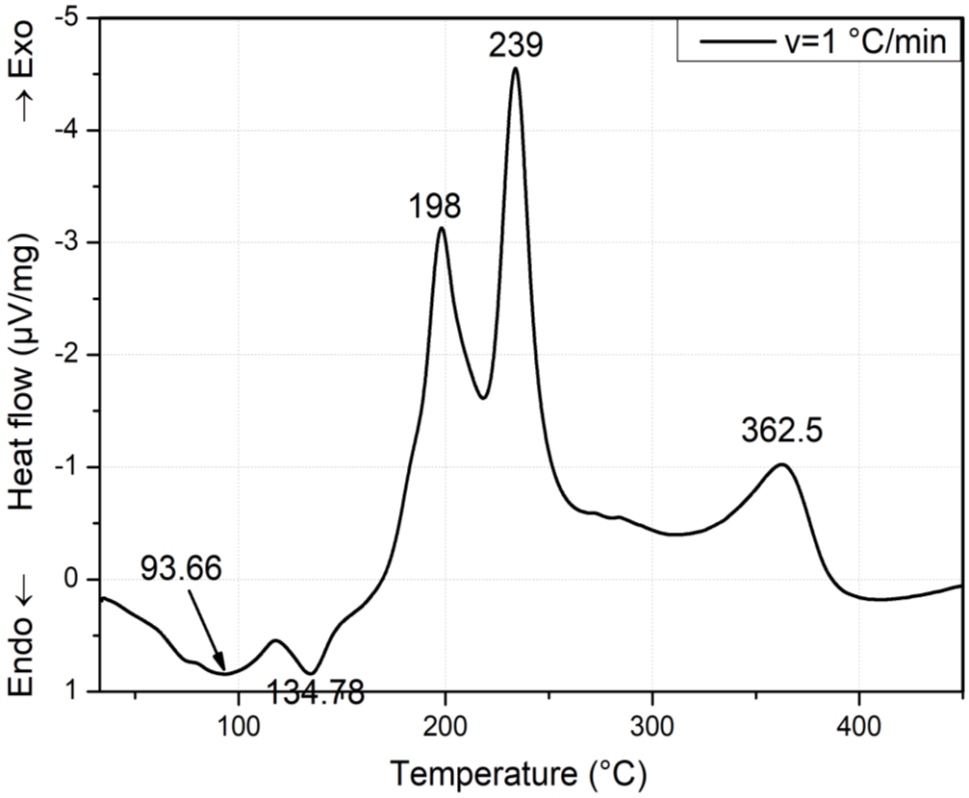

(b)

Figure (III-1): TG/DTG (a) and DTA (b) curves of powder utilized in the synthesis of $La_{0.7}Mg_{0.3}MnO_3$ heated at 1°C/min.

III.3 In Situ analysis of The Gel by X-Ray

In order to verify the phase transitions that we discussed earlier, particularly the final phase transition leading to the formation of La0.7Mg0.3MnO3, we performed X-ray analysis on the gal powder after subjecting it to various temperatures, followed by cooling and examination by x-ray diffraction **Figure (III-2).**

The diffraction curves revealed that up until a temperature of 260°C, there were no peaks, indicating the absence of a crystalline phase. This observation supports our earlier assertion that the formation of the La0.7Mg0.3MnO3 phase had not yet begun to occur. Moreover, the curves demonstrated that after the last peak in the differential thermal analysis (beyond 400°C), the La0.7Mg0.3MnO3 phase starts to form.. At a temperature of 600°C, there is a peak corresponding to oxide A, in addition to the remaining peaks that are attributable to compound La0.7Mg0.3MnO3. As the temperature increases, the diffraction peaks become more pronounced.

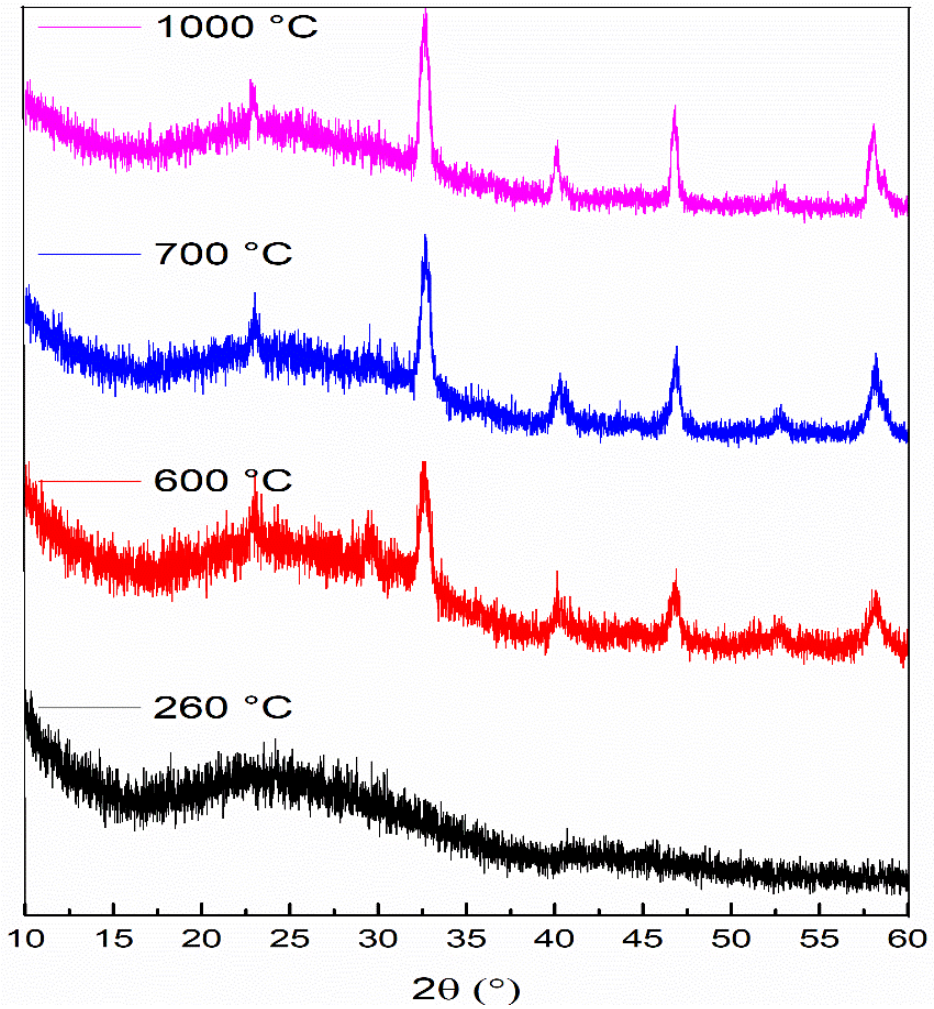

Figure (III-2) XRD spectra obtained for $La_{0.7}Mg_{0.3}MnO_3$ heated to the specified temperatures in the DTA and, then, cooled to room temperature

III.4 Effect of Heating Rate on Phase Transformations and Reaction Kinetics

The rate of heat treatment plays a crucial role in the results of Differential Thermal Analysis (DTA), influencing peak sharpness, detection of thermal phase transformation, and reaction kinetics. Faster heating rates typically result in sharper and slightly higher positioned peaks on the DTA curve, slower heating rates enable the detection of minor thermal phase transformation and differentiation of measures at close temperatures that might merge into a single peak at rapid heating. Reaction kinetics are also affected; kinetically hindered reactions may not be observed at high heating rates, while thermodynamically unfavorable reactions at low temperatures might escape detection at slow rates. The ideal heating rate, therefore, balances these aspects according to the experiment's objectives, allowing precise detection and resolution of thermal events without excessively prolonging the experiment or missing certain reactions. It's essential to specify the heating rate when comparing or reporting DTA results, given the differing outcomes at different rates for the same material.

In all our experiments, we observed that whenever we employed a heating rate exceeding 5 °C/min, an explosion ensued within the alumina crucible between temperatures of 200 and 300 °C. This phenomenon rendered tracking phase transitions unfeasible due to the displacement of the mass from its carrier. As a result, we opted for a significantly reduced heating rate for our experiments. The figure (III-3) shows the results of thermal analysis for different heating rates, in the thermal analysis results, the different regions A, B, and C represent various stages of reactions or phase transformations that happen under heat treatment for $La_{0.7}Mg_{0.3}MnO_3$.

Region A represents the stage where adsorbed water and the water contained within citric acid evaporate. The observation from Figure III-3 indicates that as the heating rate increases, the temperature at which this evaporation occurs also increases. This could be because a faster heating rate reduces the time available for evaporation to occur at a given temperature, pushing the process to a higher temperature range.

Region B represents the stage where dissociation of citric acid and nitrate happens. Just like with the evaporation of water, the dissociation temperature of these compounds also increases with the heating rate. Again, this is likely due to faster heating rates causing the system to reach equilibrium at higher temperatures.

Region C showcases the stage where a new phase starts to form. When the heating rate increases from 0.3 to 1°C/min, the phase formation temperature also increases from 343°C to 363°C. This suggests that the time it takes for the new phase to form is sensitive to the heating rate. Faster heating rates push the phase formation to occur at higher temperatures, as is clearly shown in Figure (II-4).

In summary, these observations suggest that the heating rate during thermal treatment can significantly impact the temperature at which different processes (like evaporation, dissociation, and phase formation) occur.

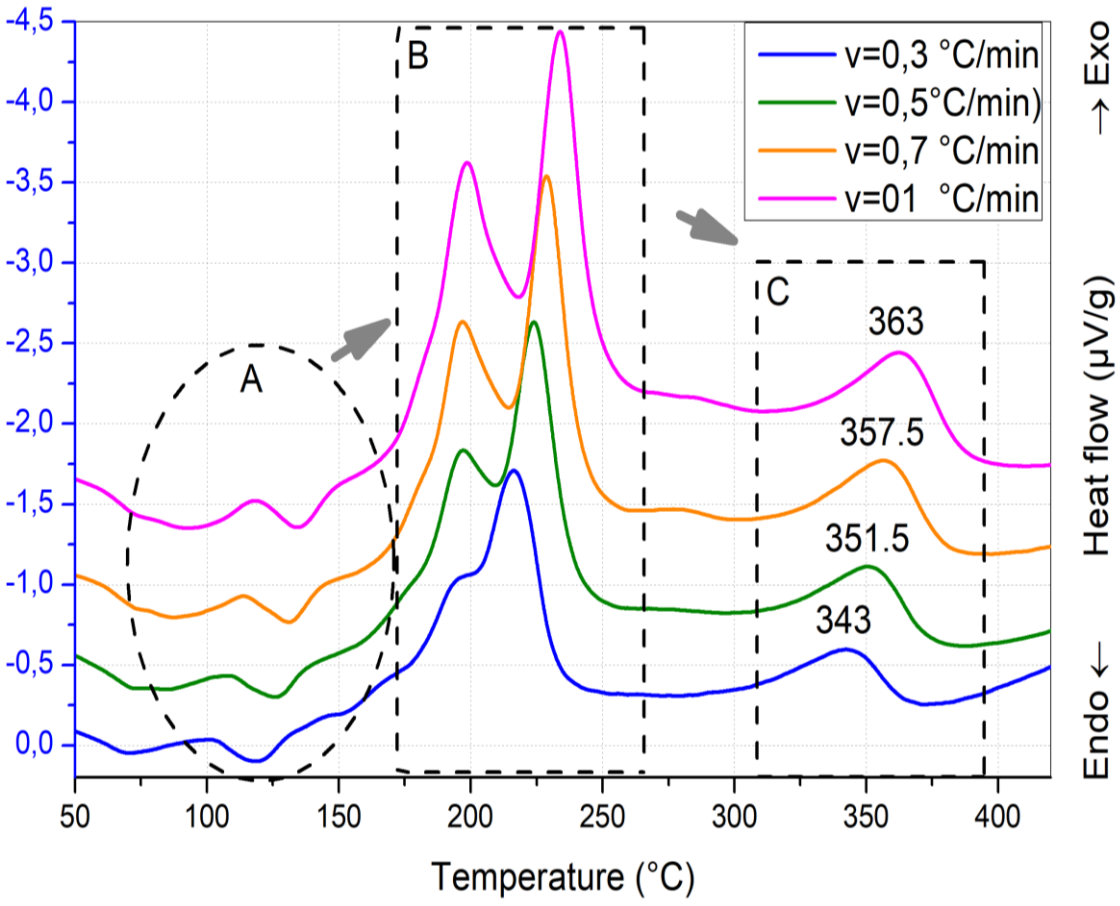

Figure (III-3): DTA curves of the powder utilized in the synthesis of $La_{0.7}Mg_{0.3}MnO_3$ heated at different heating rates

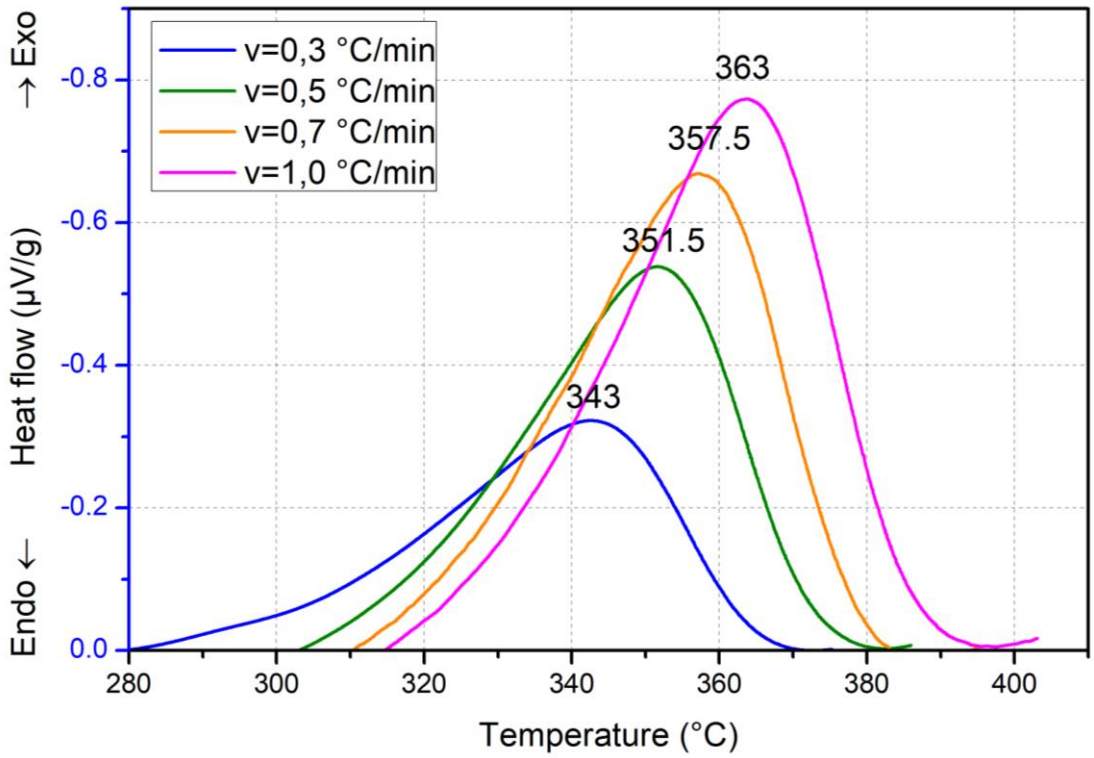

Figure (III-4): DTA curves of powder utilized in the synthesis of $La_{0.7}Mg_{0.3}MnO_3$ heated at different heating rates

III.5 Crystallization Kinetics

Introduction: Thermal analysis technique is one of the most important techniques through which we can understand the mechanism of phase transformations in solid-state. It relies on measuring changes in the physical quantities of solid materials as a function of temperature. The thermal analysis technique has been used since the early 20th century, and it requires special devices called thermal analysis devices which have become a useful tool in obtaining kinetic information such as activation energy and kinetic coefficients that describe the mechanism by which these phase transformations occur (growth and nucleation mechanisms). Thermal analysis has many devices, including Thermogravimetric Analysis (TG), Differential Thermal Analysis (DTA), Differential Scanning Calorimetry (DSC), Dilatometry (DIL), Fourier Transform Infrared Spectroscopy equipped with a furnace (FTIR), and X-ray diffractometry equipped with a furnace (RX), etc.

The most important and most used thermal analysis techniques are (TG), (DTA), (DSC), and (DIL). The importance of these techniques lies in selecting the heating rate, and they are economical as they only require very small amounts of the sample being studied, of the

order of milligrams. The problem raised is how can we exploit these techniques and the curves given by thermal analysis devices in understanding and studying the kinetics of transformations and deriving the information and kinetic factors associated with them? In order to solve the problem raised, we will describe various general kinetic models through which we can study phase transformations and derive kinetic information associated with them.

III.5.1 Transformation Models and Kinetic Laws

There are two methods for thermal analysis using the techniques of (TG), (DTA), (DSC), and (DIL), namely, isothermal and non-isothermal analysis. In the case of isothermal treatment, the sample is heated rapidly, and upon reaching a certain temperature, the temperature is kept constant for a sufficient amount of time for the crystallization process to complete. After that, the heat quantity required for the crystallization process is recorded as a function of temperature or time. However, in the case of non-isothermal treatment, the sample is heated at a constant rate and the changes in length, mass, or heat quantity are recorded as a function of time or temperature. The general kinetic law that describes the kinetics of phase transformations in solid-state is given by the following relation:

$$\mathbf{d\alpha/dt = k(T) * f(\alpha)}$$

where: α: is the conversion fraction or decomposition part. Its expression varies according to the technique and type of thermal analysis.

In TG technique, the conversion fraction is the change in mass relative to the total mass.

In DiL technique, it is the change in length relative to the total length.

f(α): is a function describing the mechanism of transformation.

k(T): is the reaction rate constant is given by the Arrhenius relation:

$$\mathbf{k(T) = A * \exp(-E/RT)}$$

A: is the atomic oscillation coefficient or the frequency factor.

T: is the temperature (in K).

R: is the ideal gas constant.

E: is the activation energy.

In the case of non-isothermal treatment, there are two methods for analysis to determine some of the kinetic parameters. The first one is based on integrating equation and the second one is based on differentiating it, taking advantage of equation.

III.5.2 Linear Reaction Models: Linear Integral Isoconversional Method

We investigated the peak temperatures (T_P) associated with the crystallization of La0.7Mg0.3MnO3 phase formation by analyzing the powder's differential thermal analysis (DTA) curves. The DTA curves were obtained under different heating rates of 0.3, 0.5, 0.7, and °C min-1. Subsequently, we graphed the Y function as a function of $1/T_P$, where the Y function corresponds to the equations proposed by Kissinger[1-3], Boswell[4], and Ozawa[5], represented by functions (1), (2), and (3), respectively:

Kissinger equation: $\ln(\frac{v}{T_p^2}) = -\frac{E_a}{RT_p} + C_1$ **(1)**

Boswell equation : $\ln(\frac{v}{T_p}) = -\frac{E_a}{RT_p} + C_2$ **(2)**

Ozawa equation: : $\ln(v) = -1.0518\frac{E_a}{RT_p} + C_3$ **(3)**

where E_a: activation energy

R: ideal gas constant

T_P: transition temperature in Kelvin

Figure (5-III) represents the statement of the changes of linear functions Ln(v), ln(v/T), $Ln(v/T^2)$ in terms of the reciprocal of temperature 1/Tp, after calculating the slope of the previous linear functions and matching it with the equations for the activation energy. We determine the E_a values shown in Table **(III-1)**. The average value of the activation energy is in the range of 186.24 kJ/mol.

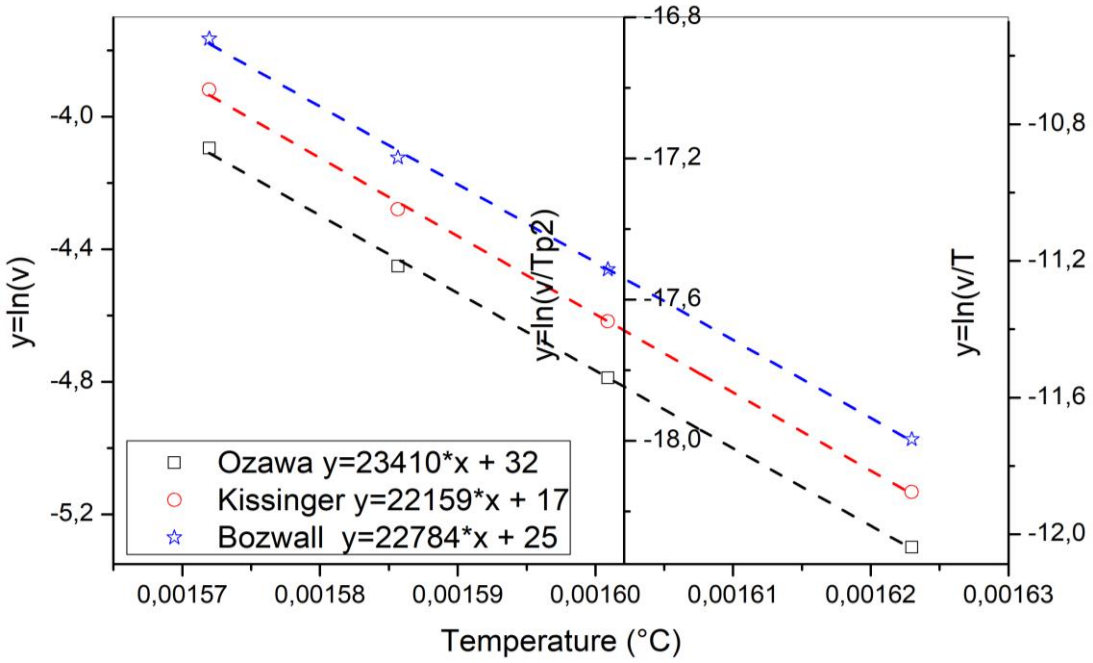

Figure (III-5): Plots of Y versus ($1/T_p$) of $\mathbf{La_{0.7}Mg_{0.3}MnO_3}$ formation at various heating rates.

Table (III-1): Activation energy values for $La_{0.7}Mg_{0.3}MnO_3$ formation

Method	**Kissinger**	**Boswell**	**Ozawa**
Activation energy E_a (kJ/mol)	184,23	189,43	185,05

We also calculated the nucleation coefficient, which is called the Avramian coefficient or the morphological growth coefficient n[6, 7] , using equation (4):

$$\mathbf{n} = \frac{2.5RT_p^2}{\Delta T_p E_a} \qquad \textbf{(4)}$$

Where we have recorded the data in Table (**III-2**), the average value of the Avrami coefficient is about 1.330 for the analysis, and this value is close to the value 1.5, which indicates that the growth process for the formation and crystallization of $La_{0.7}Mg_{0.3}MnO_3$ is growth by diffusion.

Table (III-2): Avrami coefficient values for different heating rates.

Heating rates (°C/min)	**0.3**	**0.5**	**0.7**	**1**
ΔT (°C)	34.93	32.82	32.71	32.99
T_p (°C)	343	351.5	357.5	363
Avram's coefficient	1.23	1.34	1.37	1.38

According to the **Matusita** equation shown in function (5):

$$\mathbf{Ln}\left(\frac{v^n}{T_p^2}\right) = \mathbf{C_4} - \frac{mE_a}{RT_p} \qquad \textbf{(5)}$$

We plotted the function $Ln(\frac{v^n}{T_p^2})$ in terms of $1/T_p$, as shown in Figures (III-6), to calculate the numerical coefficient, m, is mainly related to the crystal growth dimensions. The representation of the function gives a straight line and by its slope. We obtained the following value: 28417 , from which we find that the values of the Avrami coefficients n and m are about 1.5, indicating that the dominant particle growth mechanism during crystallization is three-dimensional volume diffusion with a constant number of nuclei [9].

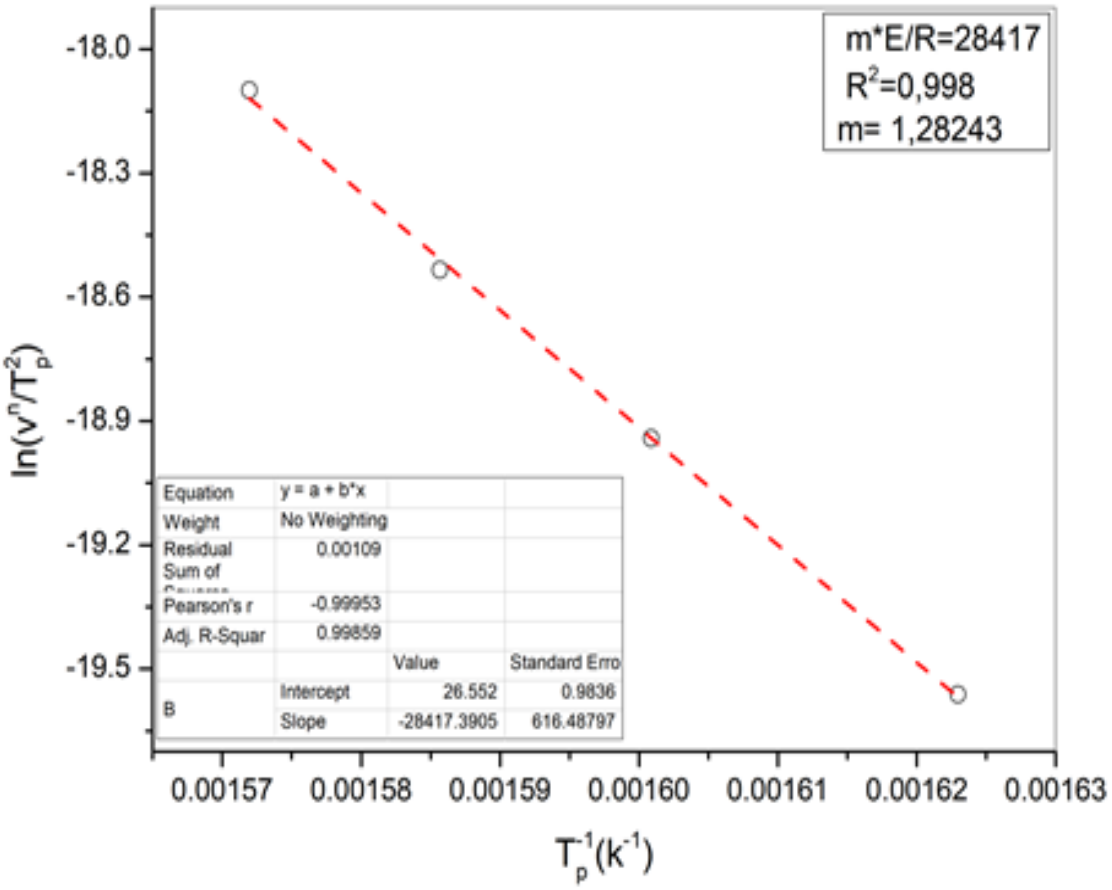

Figure (III-6): Plot of Ln($\frac{v^n}{T_p^2}$) versus $1/T_p$ according to Matusita equation

III.5.3 Linear Reaction Models: Differential Iso-Conversional Methods

to calculate the crystallization Fraction, we plot Crystallized fraction of $La_{0.7}Mg_{0.3}MnO_3$ compound fromation under different heating rates and the rate Crystallized fraction (dx/dt) a function of temperature **Figure (III-7)** for the different heating rates. In thermal transformation, we notice that the maximum transformation temperature of crystallization increases from 343 to 363°C, and it increases with increasing heating rates from 0.3 to 1°C/min, meaning that the increase in the formation rate of $La_{0.7}Mg_{0.3}MnO_3$ increases with increasing heating rate.

Based on the data of the previous curves as proposed by **Legero [10]**, after plotting the changes of ln (dx/dt) and the changes of the inverse temperature in terms of the $La_{0.7}Mg_{0.3}MnO_3$ crystallization ratio as shown in Figures **(III-8)** and (**III-9**) respectively.

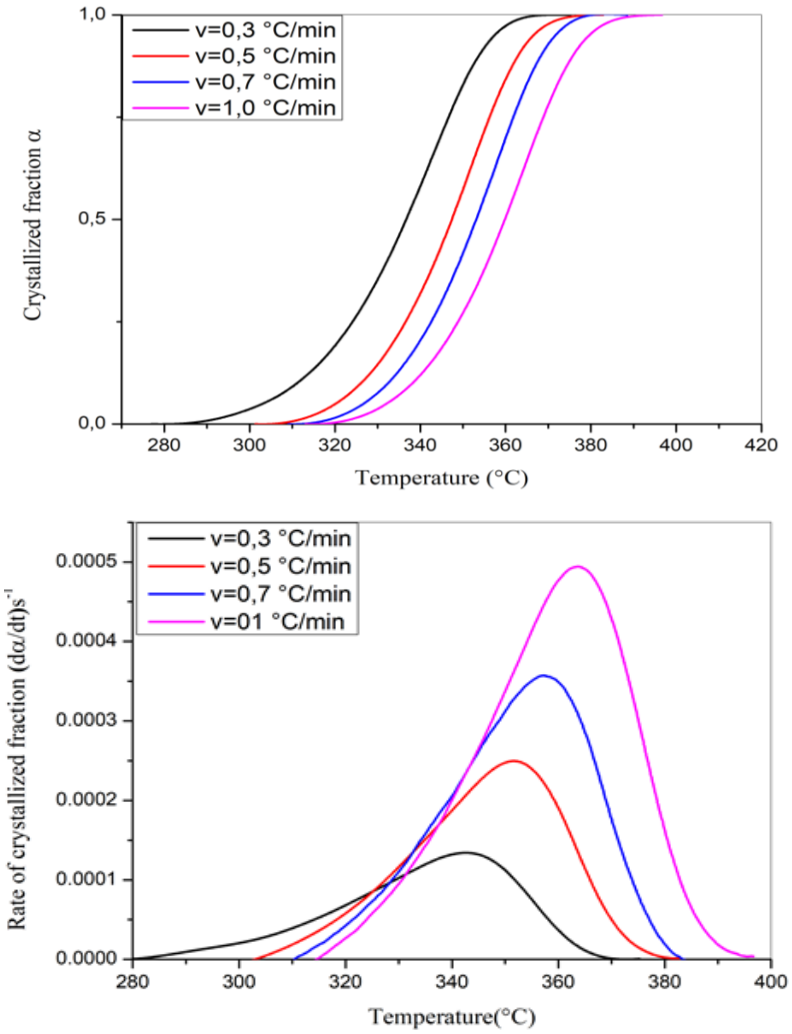

Figure (III-7): Crystallized/rate Crystallized fraction of $La_{0.7}Mg_{0.3}MnO_3$ compound fromation under different heating rates.

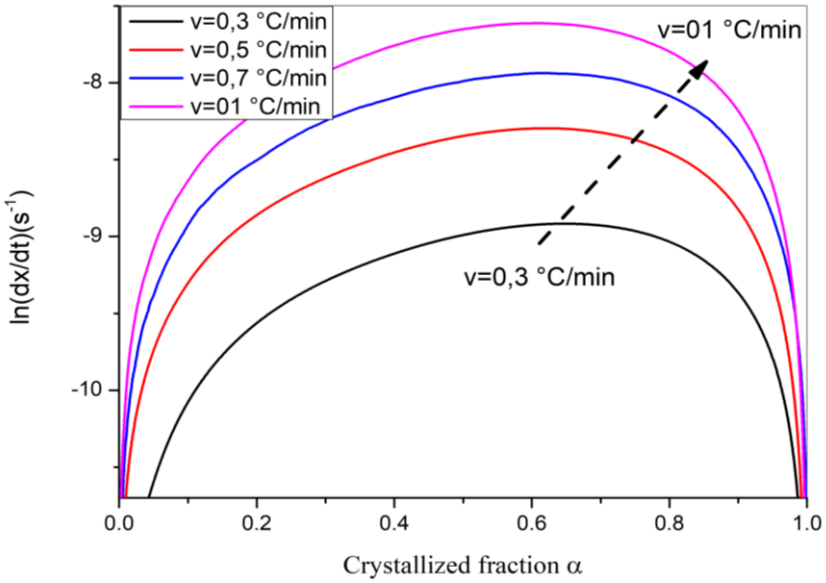

Figure (III-8): Plot of Y = ln(dx/dt) versus of crystallized fraction x at different heating rates

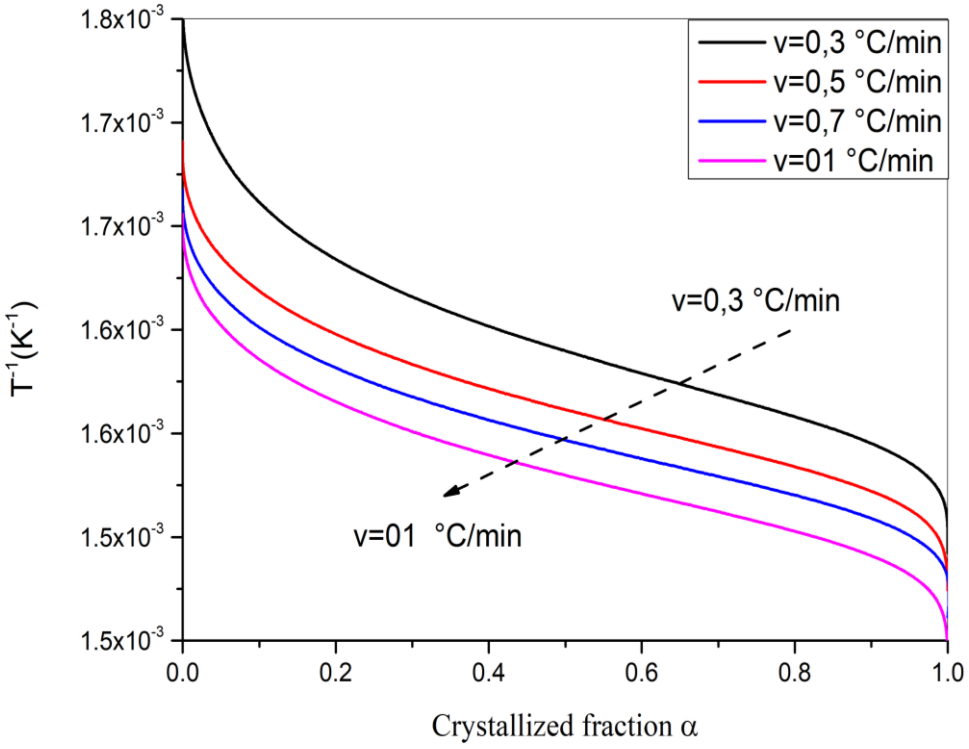

Figure (III-9): Plot of Y = 1/T versus of crystallized fraction x at different heating rates.

We plotted the function ln(dx/dt) a function of 1/T for specific values of the fraction of $La_{0.7}Mg_{0.3}MnO_3$ quantity in each experiment, with different heating rates.. Crystallization ratio values were taken in the range of 0.1 to 0.9.

$$ln\left(\frac{dx}{dt}\right) = ln[k_0 n] + \frac{n-1}{n} ln[-ln(1-x)] + ln(1-x) - \frac{E_a}{RT_m} = ln[k_0 f(x)] - \frac{E_a}{RT_p}$$

(6)

We calculate the formation energy of $La_{0.7}Mg_{0.3}MnO_3$ by plotting ln(dx/dt) as a function of 1/T for specific values of the crystalline ratio of $La_{0.7}Mg_{0.3}MnO_3$ and for different heating rates, as shown in Figure **(III-10)**. The function curves are represented by straight lines with a slope from which we calculate the activation energy, and from there we obtain the values listed in Table **III-3** below. The average activation energy value for the formation of $La_{0.7}Mg_{0.3}MnO_3$ resulting from the reaction of La, Mg and Mn oxides using differential thermal analysis was 180.71 kJ/mol. By knowing the activation energy values, we can plot the function ln[k0 f(x)] at heating rates of 0.3, 0.5, 0.7, and 1 °C/min, as a function of different ratios of $La_{0.7}Mg_{0.3}MnO_3$ quantities formed using differential thermal analysis, as shown in Figure **(III-11)**.

Table III-3: $La_{0.7}Mg_{0.3}MnO_3$ formation energy values for different crystallinity ratios

x	**0.1**	**0.2**	**0.3**	**0.4**	**0.5**	**0.6**	**0.7**	**0.8**	**0.9**
Ea (kJ/mol)	158,01	166,84	175,36	182,28	186,65	190,11	191,12	189,84	186,18
R^2	0,998	0,999	0,998	0,999	0,998	0,997	0,994	0,988	0,978

In order to calculate the Avramian coefficient of crystallization, n, we have determined many pairs of the amount of crystallization x_1 and x_2 that fulfill the equation $\ln[k_0 f(x_1)] = \ln[k_0 f(x_2)]$, and using equation (6) we get The following equation (7):

$$n = \frac{\ln\left[\ln(1-x_1)/\ln(1-x_2)\right]}{\ln\left[(1-x_1)\ln(1-x_1)/(1-x_2)\ln(1-x_2)\right]} \qquad \textbf{(7)}$$

$$\ln\left[k_0 f(x_1)\right] = \ln(k_0) + \ln(n) + \frac{n-1}{n}\left[\ln\left(-\ln(1-x)\right)\right] + \ln(1-x) \qquad (8)$$

The values of the Avrami coefficients as well as the frequency factor k_0 calculated from relation (8) for different heating rates, are listed in Table (III-4), where the average values of the Avrami coefficients using differential thermal analysis were equal to 1.27608 , Which demonstrates that the formation of $La_{0.7}Mg_{0.3}MnO_3$ occurs via volumetric diffusion. Using differential thermal analysis, the frequency factor has an average value of 11*log(6.9587)

Table (4-III): Values of Avrami coefficients and frequency factors using DTA

Heatingrates(°C/min)		0.5	1
DTA	n	1.2736	1.2784
	$k_0(10^{11})$	7.40836	6.50905

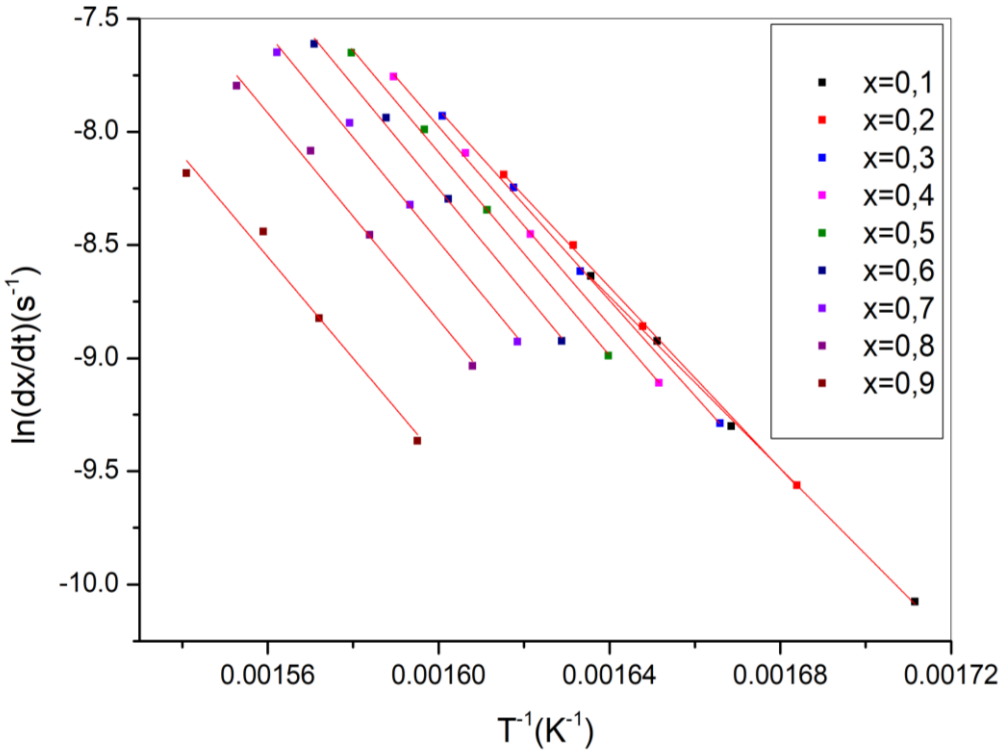

Figure (III-10): ln (dx/dt) versus 1/T at same value of crystallized fraction x at different heiting rates..

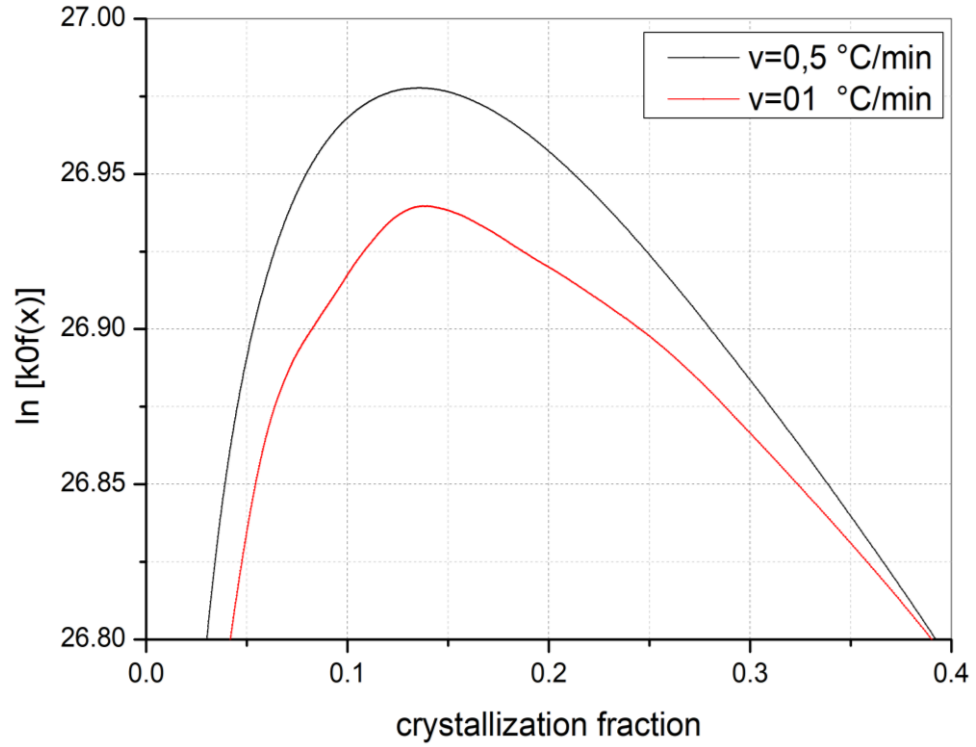

Figure (III-11): Plot of ln [$k_0 f(x)$] versus crystallization fraction for $La_{0.7}Mg_{0.3}MnO_3$ powder heated at different heating rates..

III.6. The Effect of Sintering Temperature on The Structure and Crystal Parametres of $La_{(1-X)}Mg_xMnO_3$

In our investigation of the $La_{(1-x)}Mg_xMnO_3$ compound, we varied the doping level x of the element magnesium (Mg) at the lanthanum sites. The different values of x used were 0, 0.1, 0.2, 0.3, and 0.4. We obtained a quantity of this powder and subjected it to calcined treatment for 4 hours at various temperatures: 700°C, 800°C, 900°C, 1000°C, and 1100°C. After the thermal treatment, the powder was analyzed using X-ray diffraction (XRD) equipment. Figure **(III-12)** displays the XRD spectrum of the powder after the treatment at specified temperatures, revealing the following observations **Table (III-5)**

- the formation of the phase At 700 °C, we find that the structure is orthorhombic with a space group Pnma, similar at 800°C.

-At a temperature of 900°C,1000°C and 1100°C, we found that the structure is hexagonal with a space group R-3C.

Table (III-5): space group and crystal parameters a founction of caltination temperateurs

X	700°C	800°C	900°C	1000°C	1100°C
0	Orthorhombic a=5.48 b=5.511 c=7.776	Orthorhombic a=5.473 b=5.519 c=7.783	Hexagonal a=5.527 c=13.39	Hexagonal a=5.552 c=13.46	Hexagonal a=5.514 c=13.49
0.1	Orthorhombic a=5.488 b=5.3979 c=7.85	Orthorhombic a=5.49 b=5.5289 c=7.8988	Hexagonal a=5.5193 c=13.2931	Hexagonal a=5.5237 c=13.3088	Hexagonal a=5.5119 c=13.3138
0.2	Orthorhombic a=5.50 b=5.4831 c=7.773	Orthorhombic a=5.4853 b=5.5228 c=7.937	Hexagonal a=5.5215 c=13.3355	Hexagonal a=5.5235 c=13.3238	Hexagonal a=5.5162 c=13.3233
0.3	Orthorhombic a=5.485 b=7.8846 c=5.5026	Orthorhombic a=5.5099 b=5.5111 c=7.88	Hexagonal a=5.5259 c=13.3013	Hexagonal a=5.4968 c=13.4987	Hexagonal a=5.5293 c=13.2070
0.4	Orthorhombic a=5.4918 b=5.4802 c=7.8416	Orthorhombic a=5.498 b=5.494 c=7.869	Hexagonal a=5.54 c=13.37	Hexagonal a=5.5173 c=13.4763	Hexagonal a=5.5268 c=13.5011

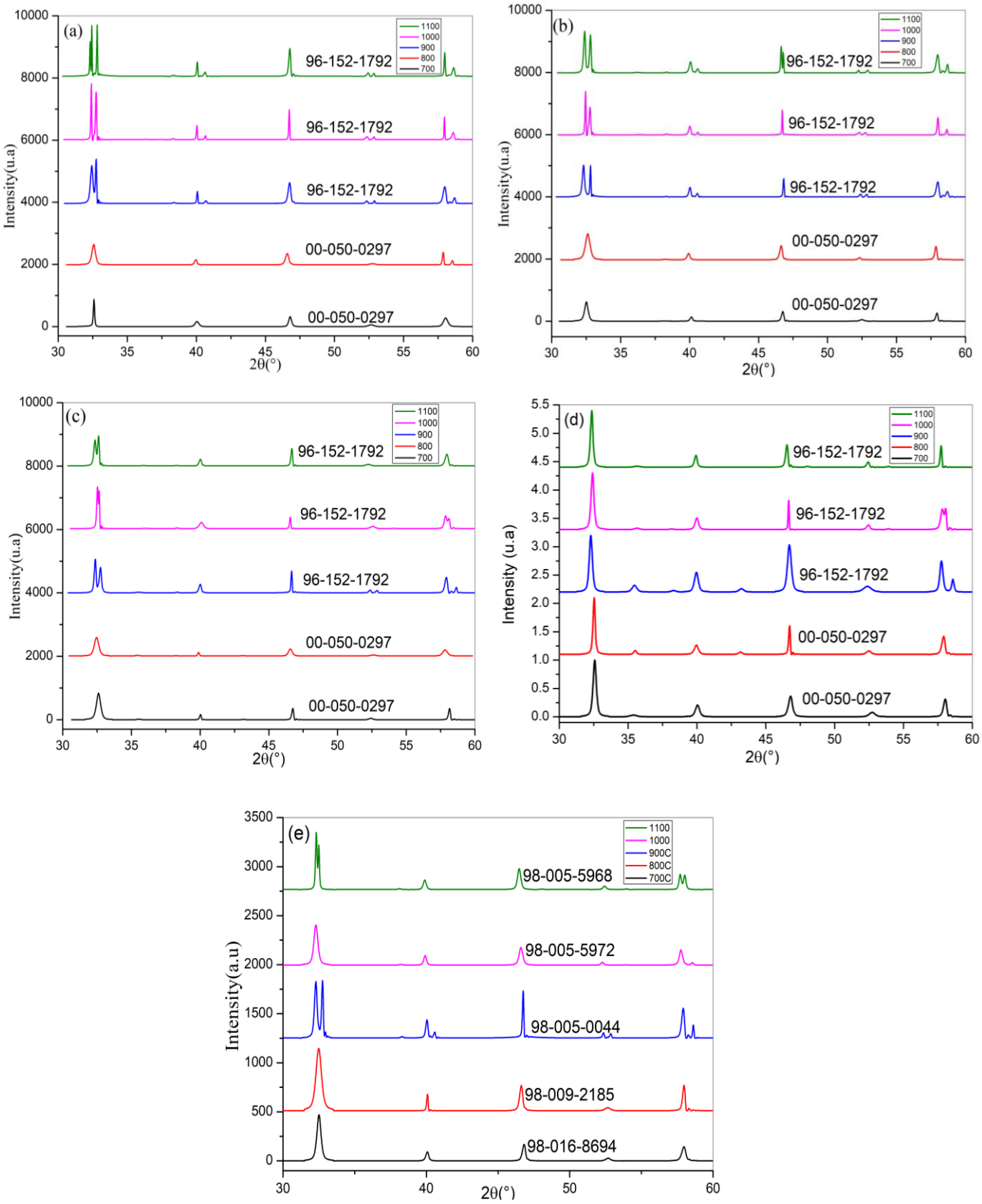

Figure (III-12): X-ray diffraction spectrum of the powder after treatment for 4 hours at different temperatures where (a) x=0.1 /(b) x=0.2 / (c) x=0.3 / (d) x=0.4 and (e) =0 .

III.7. Crystallite Size (from XRD data)

The Crystallite Size D has been calculated by applying Scherrer's equation as[11]:

$$D = \frac{K\,\lambda}{\beta_{hkl}\ \cos\theta_{hkl}} \qquad (9)$$

Where: K= 0.95 Shape facteur

λ= 0.154 nm (X- ray wavelength)

β_{hkl} = half -width of the diffraction band (FWHM)

θ_{hkl} = Bragg-diffraction angle (peak position in radians)

The preparation method we followed for synthesizing perovskite compounds allowed us to obtain a nanopowder.Whether at a temperature of 700 and then up to 1100°C and the order of the crystallite size changes from 25 to 60 nm as shown in figure (**III**-13).

- For the compound LaMnO3, with increasing temperature, the average crystalline size increases from 30 at 700 to 60 at 900, and according to the diffraction results, the structure is rhombic straight in this range. Therefore it is logical that the size of the crystals increases with increasing temperature, indicating crystal growth.

  After this temperature, a crystal transformation occurs from the orthorhombic to the hexagonal, and this transformation is accompanied by the nucleation and growth of crystals. This is why a decrease in the crystalline dimension occurs after 900 °C ,and after that, crystal growth takes place.
- Regarding the 0.4 concentration in the range from 700 to 900 °C, it behaves similarly to the 0 concentration, with the observation that the crystalline dimension is slightly lower than that of the x= 0 . At 700, the average crystalline dimension is 25 instead of 30 for the 0 concentration. This difference increases with an increase in temperature. At 900, the average crystalline dimension for x= 0.4 is 40 nanometers instead of 60 for x = 0 . This can be explained by the inhibitory role of magnesium atoms in crystal growth. The higher the concentration of magnesium, the slower the growth rate becomes.

  After the temperature of 900 °C, magnesium plays an inverse role in the hexagonal structure.
- Generally, the average crystalline dimension stabilizes between 40 and 60 for all concentrations.

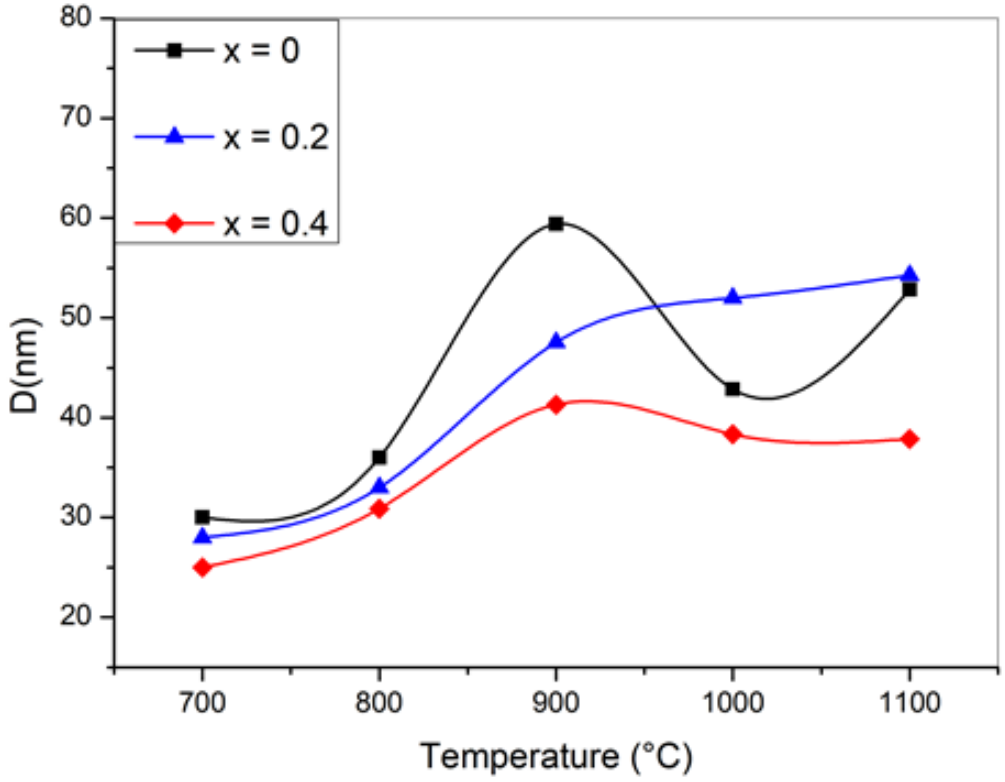

Figure (III-13): Crystallite Size

III.8.Tolerance Factor

The crystal structure could be estimated by the Goldschmidt tolerance factor (t). Later, it was used to measure the degree of distortion of a perovskite. The following equation for the Goldschmidt tolerance factor is:

$$t = \frac{(x-1)R_{La^{3+}} + xR_{Mg^{2+}} + R_{O^{2-}}}{\sqrt{2}(xR_{Mn^{+4}} + (1-x)R_{Mn^{+3}} + R_{O^{2-}})} \qquad (10)$$

The ionic radii for (La^{3+} ,Mg^{2}+,Mn^{3+} ,$Mn^{4+}$and O^{2-}) were (1.36 , 0.57 ,0.645 , 0.53 and 1.4 A°) respectively . the value of tolerance factor (t) was found to be around 0.91 and thereby confirms their distorted perovskite structure, as shown in Table III-6 and figure (III-14).

Table III-6 : Tolerance Factor values for different concentrations of Mg.

x	0	0.1	0.2	0.3	0.4
t	0.9543	0.9323	0.9099	0.8874	0.8665

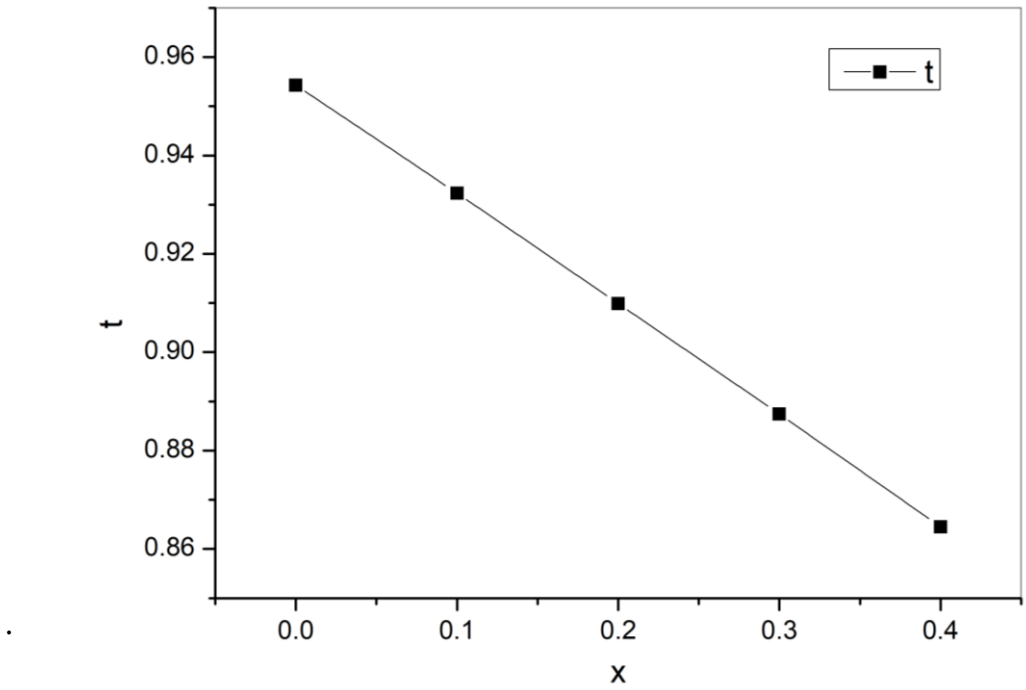

Figure (III-14): Tolerance Factor values for different concentrations of Mg.

III.9. Coefficient of Linear Expansion of $La_{0.7}Mg_{0.3}MnO_3$ by In Situ XRD Study and Dilatometry Study

In situ XRD (X-ray diffraction) is a technique used to study the structural changes of a material under various conditions, such as temperature, pressure, or gas environment. It provides valuable information about the crystal structure, phase transitions, and phase composition of a material. Some examples of structural changes that can be investigated using in situ XRD include[12]:

- **Phase Transitions**: In situ XRD can capture phase transitions, which involve the transformation of a material from one crystal structure to another. For example, it can monitor the transition from an amorphous phase to a crystalline phase, or from one crystal structure to another due to changes in temperature or pressure.

- **Crystal Growth**: In situ XRD is valuable for studying crystal growth processes. By continuously monitoring the diffraction pattern during the growth of a crystal, researchers can gain insights into the kinetics and mechanisms of crystal nucleation and growth.
- **Structural Transformations**: In some cases, materials can undergo reversible or irreversible changes in their crystal structure under specific conditions. In situ XRD can capture such structural transformations, providing information about the nature and dynamics of these changes.
- **Phase Diagrams**: In situ XRD can be used to construct phase diagrams, which depict the stable phases of a material as a function of temperature, pressure, or other variables. By systematically varying the conditions and analyzing the resulting diffraction patterns, researchers can map out the boundaries between different phases.
- **Stress and Strain Analysis:** In situ XRD can also be applied to investigate the effects of mechanical stress or strain on the crystal structure of a material. By subjecting the sample to controlled mechanical forces while performing XRD measurements, researchers can examine how the lattice parameters and crystal orientation change in response to stress.

In situ XRD (X-ray diffraction) can be used to determine the dilatation coefficient or thermal expansion coefficient of a material. The dilatation coefficient is a measure of how a material expands or contracts in response to changes in temperature. It quantifies the fractional change in length, area, or volume per degree of temperature change[13].

To determine the dilatation coefficient using in situ XRD, the sample is subjected to controlled temperature variations while X-ray diffraction measurements are performed. By analyzing the changes in the diffraction pattern as the sample expands or contracts, researchers can calculate the dilatation coefficient.

The dilatation coefficient can be determined in different ways depending on the type of measurement and the specific properties of the material being studied.

Lattice Parameter Analysis: In situ XRD can be used to measure the lattice parameters of a crystal as a function of temperature. The lattice parameter is the characteristic length of the crystal structure. By monitoring the changes in lattice parameters with temperature,

researchers can calculate the dilatation coefficient using the formula: $\alpha = (1/a) \times (da/dT)$, where α is the dilatation coefficient, a is the lattice parameter, and da/dT is the rate of change of the lattice parameter with temperature.

Powder Diffraction Analysis: For polycrystalline materials, in situ XRD can be used to analyze the changes in the diffraction pattern as a function of temperature. By fitting the diffraction peaks and determining their shifts, researchers can extract the dilatation coefficient using the Bragg equation and known crystallographic information.

It's important to note that the dilatation coefficient can vary with temperature and may also depend on the crystallographic direction within the material. Therefore, multiple measurements at different temperatures and crystallographic orientations may be necessary to obtain an accurate determination of the dilatation coefficient.

In situ XRD provides a powerful technique for investigating the thermal expansion behavior of materials and obtaining precise measurements of the dilatation coefficient. This information is valuable for understanding the response of materials to temperature changes and is relevant in various fields, including materials science, solid-state physics, and engineering.

To investigate the structural transformations and changes in lattice constants with temperature, we conducted a thermal X-ray diffraction analysis. An analysis was performed at temperatures of 700, 800, 900, and 1000°C. Additionally, we cooled the powder using a High-Temperature X-ray Diffraction (HTK XRD) equipment.

The experimental conditions involved heating at rate of 10 °C/min followed by a 20 minute hold at the analysis temperatures. X-ray diffraction measurements were then conducted immediately for a duration of 2 minutes.

Figure (III-15) shows the effect of temperature on the diffraction spectrum. It can be concluded that the crystalline structure remains stable until 900°C and was orthorhombic, which means that 20 min is not sufficient for transformation at 900°C. If the period was longer and sufficient, the structure would transform. Then the structure becomes hexagonal and remains so when cooling. Figure (III-15) shows that with increasing temperature, the diffraction angle for different crystal planes decreases, and this shows the effect of temperature on the crystal dimension. As the temperature increases, the crystalline dimensions expand, and thus the diffraction angle decreases.

Figure (III-16) illustrates the effect of heat treatment temperature on the bending angle for the crystal planes (022) and (202) in the orthorhombic structure, and their counterparts (202) and (204) in the hexagonal structure. Using the HighScore Plus software, we inferred that the crystalline structure of the powder at different temperatures (ranging from 700°C to 900°C) matches the compound LaMnO3, identified by the code 98-008-2226. Its crystal structure is determined to be orthorhombic with the space group Pnma 62 and lattice parameters a=5.472 Å, b = 7.754 Å, c = 5.513 Å. At the temperature of 1000 °C and after cooling, it matches the compound LaMnO3, identified by the code 98-016-7063. Its crystal structure was determined to be hexagonal with the space group R-3c 167 and lattice parameters a=5.4910 Å, b = 5.5910 Å, c = 13.3070 Å, and $\alpha = \beta = 90$, $\gamma = 120$.

By using the Rietveld method to determine the structure and calculate the lattice parameters based on the matching with a known compound's structure and parameters, we calculated the crystal lattice constants and unit cell volume at different temperatures. We observed that with an increase in temperature, the unit cell volume increases, as indicated in Table (III-7).

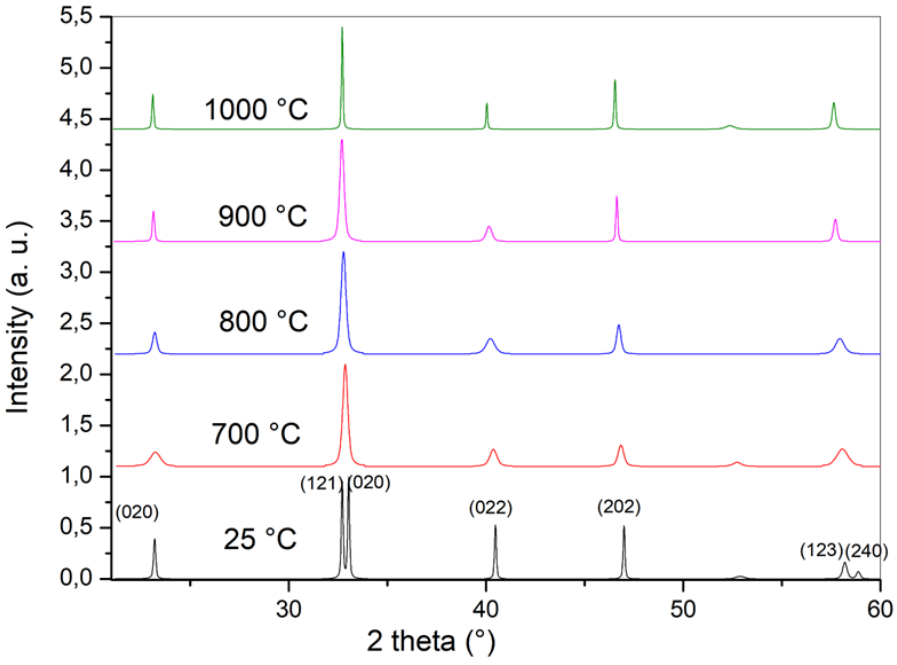

Figure (III-15): In situ XRD study of La0.7Mg0.3MnO3 Powder at Temperatures of 700, 800, 900, 1000 °C , and after Cooling for 20 minutes to each temperature, with a heating rate of 10°C/min.

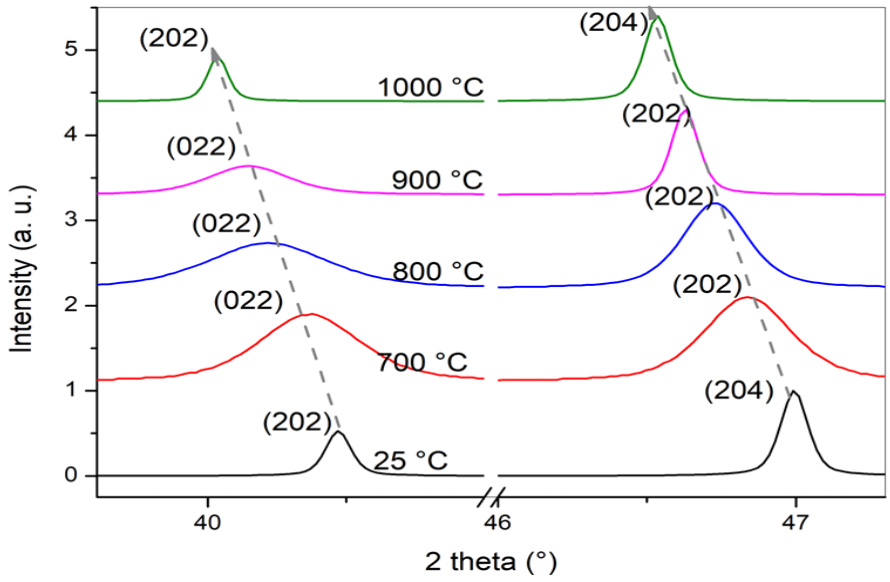

Figure (III-16): The effect of heat treatment temperature on the bending angle for the crystal planes (022) and (202) in the orthorhombic structure, and their counterparts (202) and (204) in the hexagonal structure.

Table (III-7): Coefficients of linear and volumetric expansion inferred from the Instantaneous diffraction spectrum

T	V_0	V_T	ΔT	$V_T/V0$	ΔL/L0	$\alpha.10^{-6}$	$B.10^{-6}$
1000	229.44	236.97	975	1.032819038	0.010822	11.0996	33.6606
900	229.44	234.89	875	1.023753487	0.007856	8.97823	27.1468
800	229.44	233.9	775	1.019438633	0.006438	8.30711	25.0821
700	229.44	233,24	675	1,016562064	0,005490	8.1341	24.5364

The coefficients of linear and volumetric expansion are parameters that describe a material's response to changes in temperature and pressure. In the case of the compound La0.7Mg0.3MnO3, the linear expansion coefficient can be calculated by measuring the change in the length of the crystal structure constants with respect to temperature variations. The volumetric expansion coefficient represents the change in volume of the material with respect to temperature. The values of the linear and volumetric expansion

coefficients for the LaMnO3 compound are essential information for understanding the material's behavior under different conditions, such as thermal expansion, thermal contraction, and pressure response. This information can be utilized in various applications, such as electronic device design and functional materials. The linear and volumetric expansion coefficients can be calculated through two different methods: first, by relying on the results of local deflection spectroscopy analysis, and second, using a Length Expansion device. The relationship between the linear expansion coefficient and temperature can be expressed by the equation[13, 14]:

$$\alpha = (\Delta L / L_o) / \Delta T \qquad (11)$$

Where : α :The coefficient of linear expansion .

ΔL and L_o are the change in length and the original length of the sample

ΔT : change in temperature

The relationship for the volumetric expansion coefficient is given by Equation (12):

$$\beta = (\Delta V / V_o) / \Delta T \qquad (12)$$

where: β is the volumetric expansion coefficient.

ΔV : Change in volume .

V0 : the original volume of the material.

ΔT : the change in temperature.

The relationship between the relative change in length and the relative change in volume can be described as follows:

$$(\Delta L / L_o) = (\Delta V / V_o)^{1/3}-1 \qquad (13)$$

From the previous equations , it is possible to calculate the linear and volumetric expansion coefficients of the compound at different temperatures. The results are illustrated in Table (III-7) and Figure (III-17), which show the curve of the linear expansion coefficient as a function of temperature, and Figure (III-17), which shows the curve of the volumetric expansion coefficient as a function of temperature.

By examining the table, we observe an increase in both of the linear and volumetric expansion coefficients with the rise in temperature within the studied range (700°C, 800°C, 900°C, 1000°C). The coefficient changes from a value of 8 * $10^{(-6)}$ at 700 degrees to 9 *

$10^{(-6)}$. These values are consistent with the expansion coefficients of ceramic materials. By comparing them with the coefficients of other materials, we find the following:

1. **Metals:** The thermal expansion coefficients for most common metals typically range from $5x10^{-6}$ K^{-1} to $25x10^{-6}$ K^{-1}. For example, for aluminum it's around $22x10^{-6}$ K^{-1}, for copper it's around $16x10^{-6}$ K^{-1}, and for steel, it's around $12x10^{-6}$ K^{-1}. Therefore, La0.7Mg0.3MnO3, with a thermal expansion coefficient of $8x10^{-6}$ K^{-1}, would generally have a smaller thermal expansion than most common metals.
2. **Ceramics:** Ceramics usually have lower thermal expansion coefficients compared to metals, often less than $5x10^{-6}$ K^{-1}. For instance, the thermal expansion coefficient of Alumina (Al_2O_3), a widely used ceramic material, is about $9x10^{-6}$ K^{-1}. Therefore, La0.7Mg0.3MnO3 would typically have a equal thermal expansion coefficient than many ceramics[13].
3. **Polymers:** Thermal expansion coefficients for polymers can vary quite widely, from less than 10^{-6} K^{-1} to several hundreds of 10^{-6} K^{-1}, depending on the type of polymer and its crystallinity. Therefore, La0.7Mg0.3MnO3 would generally have a lower thermal expansion coefficient than most polymers[13].
4. **Glasses**: The thermal expansion coefficient of common glasses, such as soda-lime glass, is approximately $9x10^{-6}$ K^{-1}. Therefore, the thermal expansion coefficient of La0.7Mg0.3MnO3 would be similar to or slightly less than that of common glasses[13].

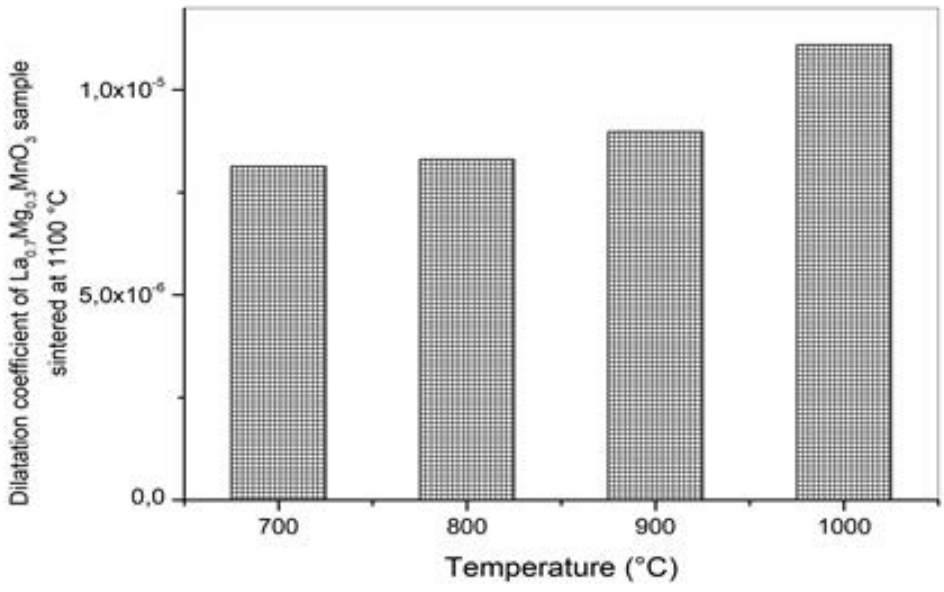

Figure (III-17): The linear expansion coefficient as a function of temperature,

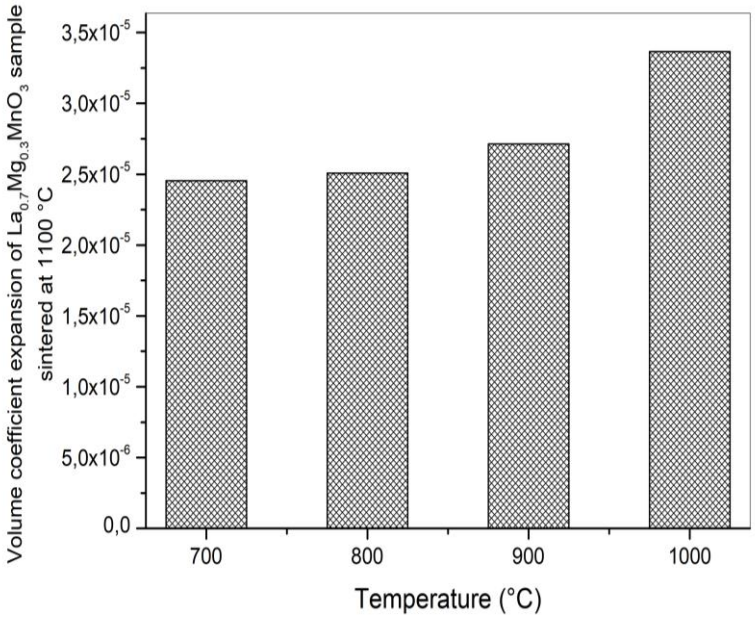

Figure (III-18): The volumetric expansion coefficient as a function of temperature.

The average value of the coefficient of linear expansion for the compound has been calculated and was approximately 8.4×10^{-6} °C^{-1} in the temperature range up to 900°C. This value closely matches the results obtained from experimental measurements. These findings are also consistent with a previous study conducted in this range[15] .

These results support our understanding of the material's behavior and the effect of temperature on its linear expansion and volume. This information contributes to determining the physical properties of the compound and understanding its behavior under different conditions. Furthermore, the agreement between experimental results and previous studies increases the credibility of the findings and confirms the validity of the work carried out in this field.

Figure (III-19) illustrates the relative change in length with respect to the initial length as a function of temperature for a sample of $La_{0.7}Mg_{0.3}MnO_3$ powder using a dilatometer. A uniaxial pressure of 100 MPa was applied during the powder compaction process, forming a cylindrical shape with a radius of 1 cm and a diameter of approximately 4 mm. A heating rate of 5°C/min was employed, and the relative change in length was calculated during the cooling process (after sintering occurred at 1100°C).
we can inferred that there is no phase transformation occurring, indicating that the compound is chemically stable. Additionally, there is no structural transformation occurring

during the cooling process, which is evident because the relative change in length is represented by a straight line with respect to temperature.

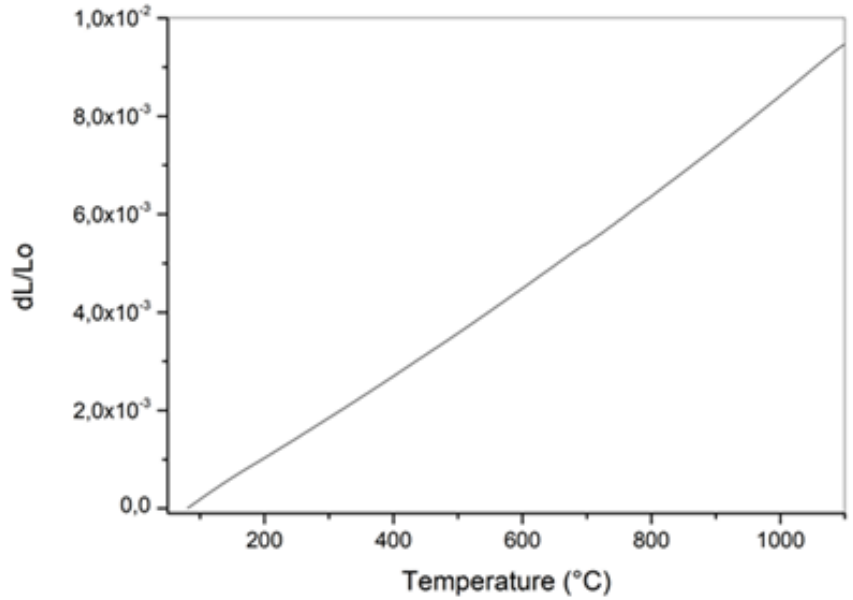

Figure (III-19): the relative linear expansion of the La0.7Mg0.3MnO3 sample with a heating rate of 5°C/min.

Figure (III-20) illustrates the function of the coefficient of linear expansion with temperature. It was evident that the value of the expansion coefficient ranges from $8.3x10^{-6}$ at lower temperatures, increasing to $10x10^{(-6)}$ at 950°C. These values are consistent with those calculated using X-ray diffraction analysis.

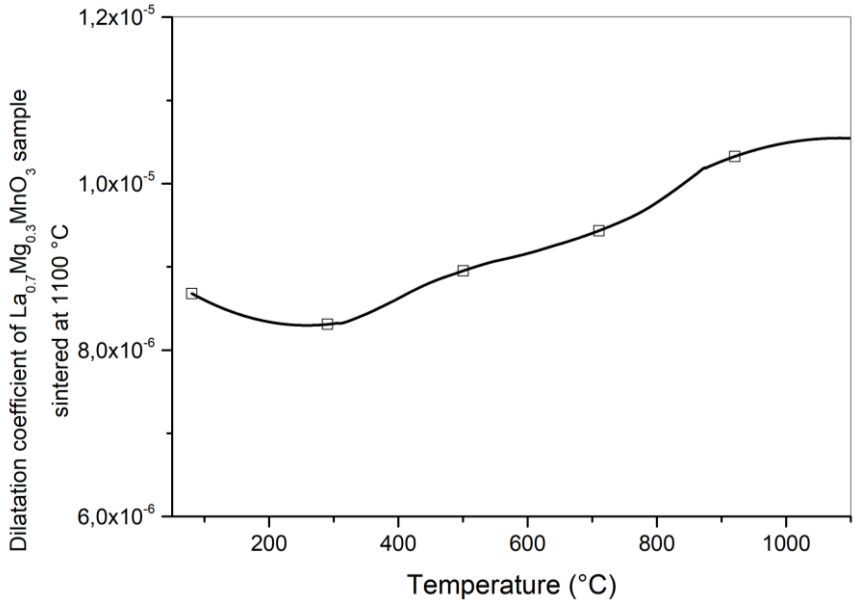

Figure (III-20): The coefficient of linear expansion, which is inferred from thermal expansion

III.10. References

1. Kissinger, H.E., *Reaction kinetics in differential thermal analysis.* Analytical chemistry, 1957. **29**(11): p. 1702-1706.
2. Coats, A.W. and J. Redfern, *Kinetic parameters from thermogravimetric data.* Nature, 1964. **201**(4914): p. 68-69.
3. Guang, Z., et al., *Kinetics of thermal decomposition of lanthanum oxalate hydrate.* Transactions of Nonferrous Metals Society of China, 2012. **22**(4): p. 925-934.
4. Boswell, P., *On the calculation of activation energies using a modified Kissinger method.* Journal of Thermal Analysis and Calorimetry, 1980. **18**(2): p. 353-358.
5. Ozawa, T., *A new method of analyzing thermogravimetric data.* Bulletin of the chemical society of Japan, 1965. **38**(11): p. 1881-1886.
6. Augis, J. and J. Bennett, *Calculation of the Avrami parameters for heterogeneous solid state reactions using a modification of the Kissinger method.* Journal of thermal analysis, 1978. **13**: p. 283-292.
7. Ray, C.S., W. Huang, and D.E. Day, *Crystallization kinetics of a lithia–silica glass: effect of sample characteristics and thermal analysis measurement techniques.* Journal of the American Ceramic Society, 1991. **74**(1): p. 60-66.
8. Matusita, K. and S. Sakka, *Kinetic study of crystallization of glass by differential thermal analysis—criterion on application of Kissinger plot.* Journal of Non-Crystalline Solids, 1980. **38**: p. 741-746.
9. Romero, M., J. Martín-Márquez, and J.M. Rincón, *Kinetic of mullite formation from a porcelain stoneware body for tiles production.* Journal of the European Ceramic Society, 2006. **26**(9): p. 1647-1652.
10. Ligero, R., et al., *A study of the crystallization kinetics of some Cu-As-Te glasses.* Journal of Materials Science, 1991. **26**: p. 211-215.
11. Mali, A. and A. Ataie, *Structural characterization of nano-crystalline BaFe12O19 powders synthesized by sol–gel combustion route.* Scripta Materialia, 2005. **53**(9): p. 1065-1070.
12. Chung, D.D., *X-ray diffraction at elevated temperatures: a method for in situ process analysis.* 1993: Wiley-VCH.
13. James, J., et al., *A review of measurement techniques for the thermal expansion coefficient of metals and alloys at elevated temperatures.* Measurement science and technology, 2001. **12**(3): p. R1.

14. Touloukian, Y., et al., *Thermophysical properties of matter-the TPRC data series. Volume 12. Thermal expansion metallic elements and alloys.(Reannouncement). Data book*. 1975, Purdue Univ., Lafayette, IN (United States). Thermophysical and Electronic ….

15. Mahata, A., P. Datta, and R.N. Basu, *Synthesis and characterization of Ca doped LaMnO3 as potential anode material for solid oxide electrolysis cells.* Ceramics International, 2017. **43**(1): p. 433-438.

Conclusion

The results presented in this work are part of investigating new materials with a perovskite structure. These materials have remarkable physical properties.

Lanthanum manganite is a compound composed of lanthanum, manganese, and oxygen. It exhibits interesting magnetic and electrical properties, making it useful in various applications.

Using a Sol-Gel method, we prepared $LaMnO_3$ doped with Mg at different concentrations (0, 0.1, 0.2, 0.3, and 0.4 %), resulting in nanopowder with crystallite dimensions ranging from 30 to 60 nanometers. The powder was characterized through various analyses, such as Thermogravimetric Analysis (TG) and Differential Thermal Analysis (DTA), and calculate the activation energy. The obtained results indicated that the Avrami coefficients n and m values are about 1.5, indicating that the dominant particle growth mechanism during crystallization is three-dimensional volume diffusion with a constant number of nuclei.

X-ray diffraction measurements at different temperatures revealed an Orthorhombic structure at 700 and 800°C, while a hexagonal structure was observed at 900,1000, and 1100 °C. The structure remained constant regardless of the Mg concentration, although there were changes in lattice constants without directly affecting the nature of the lattice.

To calculate the expansion coefficient, we used two methods, First by using dilatometric equipment and second by local analysis (to calculate the crystal lattice constants) by thermal X-ray diffraction experiment (in situ XRD, HTK-XRD) and used the coefficients expansion device. We found that the dilatation and volumetric expansion coefficients increased with temperature in the studied range (700, 800, 900, and 1000 degrees Celsius). The values changed from $8x10^{-6}$ at 700 °C to $9x10^{-6}$, which aligns with the expansion coefficients typically observed in ceramic materials.

Abstract

In this work, we have developed a series of magnetocaloric Perovskite oxide materials $La_{1-x}Mg_xMnO_3$ with x=0, 0.1, 0.2, 0.3, .and 0.4 by the sol-gel self-combustion method. Analysis of X-ray diffractograms shows that these compounds crystallize in orthorhombic structure with space group Pnma (space group number 62) at 700-800°C(t_f=4h), and at 900 to 1100°C crystallize in hexagonal structure with space group R-3c (n=167). Non-isothermal differential thermal analysis was used In order to know the phase transitions and to determine kinetic parameters for the formation of Lanthanum manganite $La_{0.7}Mg_{0.3}MnO_3$. it was calculated by linear reaction models using two methods. The first is Integral isoconversional by equations of Ozawa. Boswell, and Kissinger. The average activation energy (E_a), correlation coefficient (R^2), Avrami parameter (n), and dimensionality of crystal growth (m) were equal to 186 kJ mol^{-1}, 0.99, 1.33, and 1.28, respectively. the second is Differential isoconversional, The results show that the bulk nucleation is followed by three-dimensional growth of LMO phases with polyhedron-like morphology controlled by diffusion from a constant number of nuclei. a low coefficient of thermal expansion (CTE) of $8.4 \times 10^{-6}/\circ C$ was measured, in the range 25–900 ◦C, by In Situ XRD and Dilatometry Study.

Keywords*: Lanthanum manganite, Perovskite oxide, In Situ XRD, kinetic parameters, thermal expansion.*

ملخص

في هذا البحث قمنا بتحضير سلسلة من المواد البيروفيسكية الاوكسيدية المغناطسية $La_{1-x}Mg_xMnO_3$ مع x=0.1, 0.2, 0.3, 0.4, باستعمال طريقة ساءل هلام المرفقة بالانفجار الذاتي. بينت نتائج التحليل للمساحيق المحضرة ان البنية هي معينية مستقيمة زمرتها Pnma و رقمها هو 62 عند 700-800°C لمدة معالجة 4سا. و سداسية زمرتها R-3c و رقمها 167. استعملنا التحليل الحراري التفاضلي لمعرفة التحولات الطورية و تحديد الثوابت الحركية لتشكل الطور La0.7Mg0.3MnO3. لقد حسبنا ذلك باخذ التقريب الخطي للتفاعلات و هذا بطريقتين. الاولى و هي المكاملة و اخذنا معادلات كل من اوزاوا و بوزوال و كيسنجر. معدل طاقة التنشيط (Ea) و معامل الارتباط و ثابت افرمي (n) و معامل النمو الهندسي (m) هي 186 kJ mol^{-1} و 0.99 و 1.33 و 1.28 على الترتيب. و الثانية هي المفاضلة. النتائج بينت ان نمو بلورة LMO متعدد الوجوه في ثلاث ابعاد عن طريق الانتشار الحجمي مع ثبات عدد انوية التبلور. تم حساب معامل التمدد الطولي الصغير جدا $8.4 \times 10^{-6}/°C$ باخذ نتائج انعراج الاشعة السينية الموضعية و كذا نتائج التمدد الطولي الحراري.

الكلمات المفتاحية: *Lanthanum manganite، Perovskite oxide، In Situ XRD، kinetic parameters، thermal expansion.*